AD-A129 283 THE AFGL (AIR FORCE GEOPHYSICS LABORATORY) SPECTRAL 1/1
MODEL OF THE MOIST GL..(U) AIR FORCE GEOPHYSICS LAB
HANSCOM AFB MA S BRENNER ET AL. 16 DEC 82
UNCLASSIFIED AFGL-TR-82-0393 F/G 4/1 NL

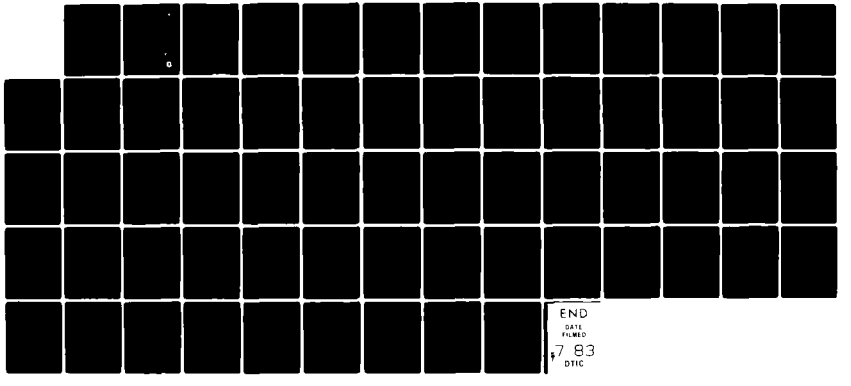

END
DATE FILMED
7 83
DTIC

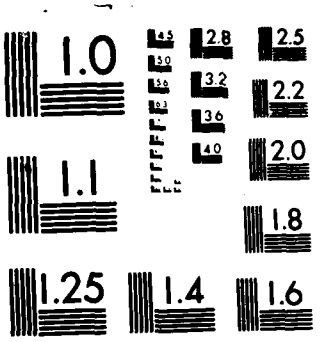


MICROCOPY RESOLUTION TEST CHART
NATIONAL BUREAU OF STANDARDS-1963-A

AFGL-TR-82-0393
ENVIRONMENTAL RESEARCH PAPERS, NO. 815

# The AFGL Spectral Model of the Moist Global Atmosphere: Documentation of the Baseline Version

STEPHEN BRENNER
CHIEN-HSIUNG YANG
SAMUEL Y.K. YEE

16 December 1982





METEOROLOGY DIVISION PROJECT 2310
AIR FORCE GEOPHYSICS LABORATORY
HANSCOM AFB, MASSACHUSETTS 01731

AIR FORCE SYSTEMS COMMAND, USAF

This report has been reviewed by the ESD Public Affairs Office (PA) and is releasable to the National Technical Information Service (NTIS).

This technical report has been reviewed and is approved for publication.

Alva T Stair, Jr.

DR. ALVA T. STAIR, Jr
Chief Scientist

Qualified requestors may obtain additional copies from the Defense Technical Information Center. All others should apply to the National Technical Information Service.

Unclassified

SECURITY CLASSIFICATION OF THIS PAGE (When Data Entered)

| REPORT DOCUMENTATION PAGE | READ INSTRUCTIONS BEFORE COMPLETING FORM |
|---|---|
| 1 REPORT NUMBER: AFGL-TR-82-0393 | 2. GOVT ACCESSION NO.: AD-A129 243 |
| | 3. RECIPIENT'S CATALOG NUMBER |
| 4 TITLE (and Subtitle): THE AFGL SPECTRAL MODEL OF THE MOIST GLOBAL ATMOSPHERE: DOCUMENTATION OF THE BASELINE VERSION | 5. TYPE OF REPORT & PERIOD COVERED: Scientific. Final. |
| | 6 PERFORMING ORG. REPORT NUMBER: ERP, No. 815 |
| 7. AUTHOR(s): Stephen Brenner, Chien-Hsiung Yang, Samuel Y.K. Yee | 8. CONTRACT OR GRANT NUMBER(s) |
| 9 PERFORMING ORGANIZATION NAME AND ADDRESS: Air Force Geophysics Laboratory (LYP), Hanscom AFB, Massachusetts 01731 | 10. PROGRAM ELEMENT, PROJECT, TASK AREA & WORK UNIT NUMBERS: 2310G701, 2310G702, 61102F |
| 11. CONTROLLING OFFICE NAME AND ADDRESS: Air Force Geophysics Laboratory (LYP), Hanscom AFB, Massachusetts 01731 | 12. REPORT DATE: 16 December 1982 |
| | 13 NUMBER OF PAGES: 65 |
| 14 MONITORING AGENCY NAME & ADDRESS(if different from Controlling Office) | 15. SECURITY CLASS. (of this report): Unclassified |
| | 15a. DECLASSIFICATION DOWNGRADING SCHEDULE |

16. DISTRIBUTION STATEMENT (of this Report)

Approved for public release; distribution unlimited.

17 DISTRIBUTION STATEMENT (of the abstract entered in Block 20, if different from Report)

18 SUPPLEMENTARY NOTES

19 KEY WORDS (Continue on reverse side if necessary and identify by block number)

Atmospheric models
Global atmospheric circulation
Numerical weather prediction
Weather forecasting
Moist atmospheric models
Spectral models

20 ABSTRACT (Continue on reverse side if necessary and identify by block number)

The baseline version of the AFGL model of the moist global atmosphere is described in detail. The numerical methods include spectral representation in the horizontal, the Arakawa vertical differencing scheme, and the semi-implicit time scheme. For this version, the pre- and postprocessing, the nonlinear normal mode initialization and the parameterized boundary layer processes and moisture physics are adapted from the NMC spectral model. A series of test forecasts indicates that the model performance is comparable to that of similar large-scale models.

DD FORM 1 JAN 73 1473 EDITION OF 1 NOV 65 IS OBSOLETE

Unclassified

SECURITY CLASSIFICATION OF THIS PAGE (When Data Entered)

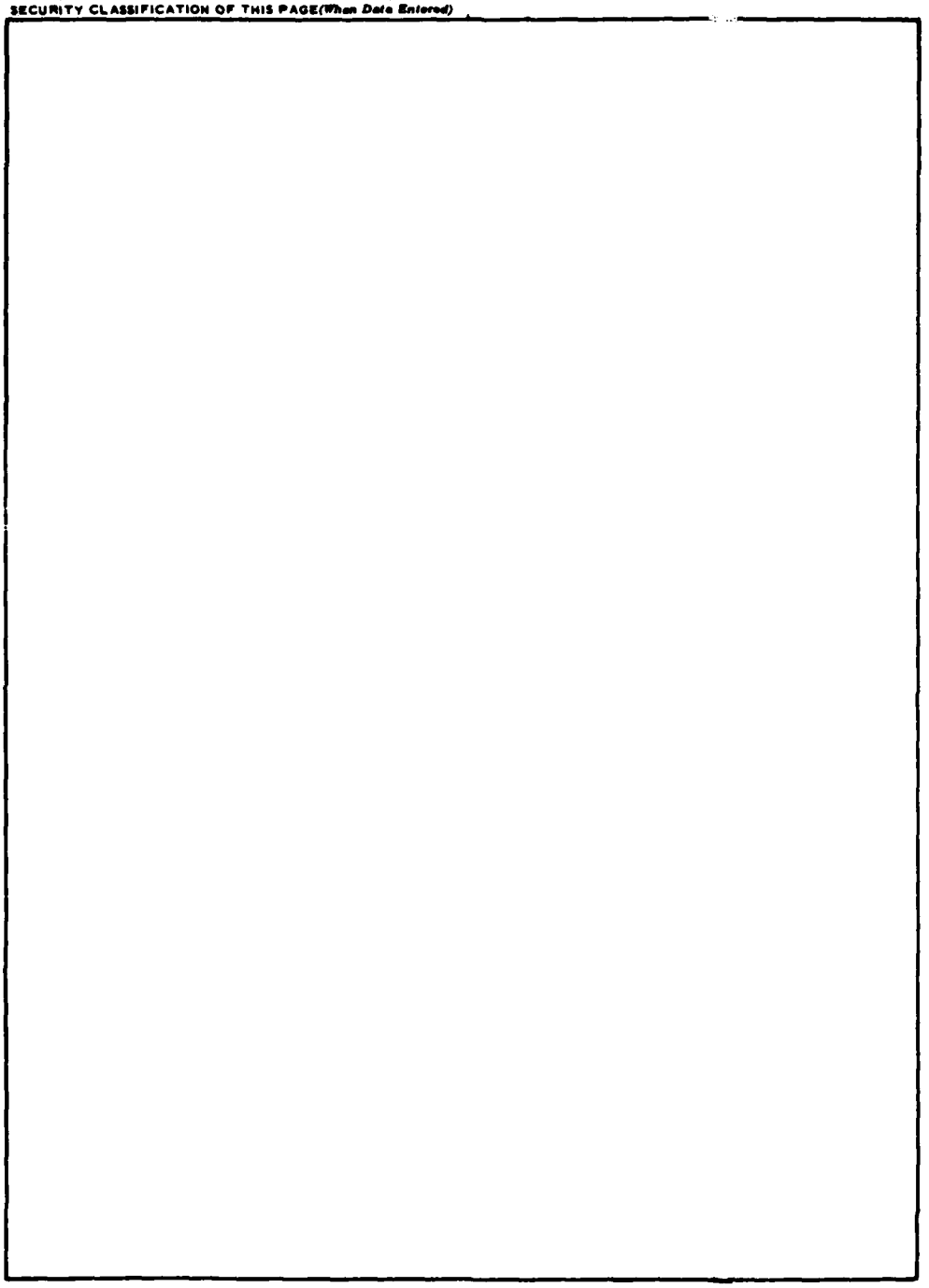

## Preface

We wish to express our deep appreciation to Dr. Joseph Sela from the National Meteorological Center (NMC) for making the code of the NMC spectral model available to us and for his many informative and helpful discussions. Dr. Bradley Ballish, also from NMC, provided us with valuable details of the normal mode initialization procedure. Dr. Isidore Halberstam, Mr. Don Nordquist, and Ms. Shu-lin Tung from Systems and Applied Sciences Corp., were instrumental in adapting the NMC initialization scheme to our model and computer system.

We would also like to thank the newest member of our group, Dr. Kenneth Mitchell, for reviewing the manuscript and for his helpful suggestions and discussions. Many thanks also go to Mr. Donald Aiken and Mr. Karekin Agazarian for their invaluable programming assistance and for deciphering and maintaining the FGGE data sets. Finally, our gratitude goes to Ms. Betty Blanchard for her infinite patience in typing the manuscript.

# Contents

## Contents



## Illustrations



## Tables

## Tables

# The AFGL Spectral Model of the Moist Global Atmosphere: Documentation of the Baseline Version

## 1. INTRODUCTION

In recent years there has been a widespread shift from finite difference methods to spectral methods in the area of numerical simulation of the global atmosphere. This change has occurred at both research centers (for example, Hoskins and Simmons[1]) and operational centers (for example, Bourke et al,[2] Sela[3]). It is due primarily to the advent of the so-called transform method (Eliasen et al,[4] Orszag[5]), which has permitted spectral methods to become competitive with finite difference methods in terms of computer time and memory requirements. In view

(Received for publication 13 December 1982)

1. Hoskins, B.J., and Simmons, A.J. (1975) A multi-layer spectral model and the semi-implicit method, Quart. J. Roy. Meteorol. Soc. 101:637-655.

2. Bourke, W., McAvaney, B., Puri, K., and Thurling, R. (1977) Spectral methods for atmospheric modeling, Methods in Computational Physics, Vol. 17. B. Adler, Ed., Academic Press, New York, pp. 267-324.

3. Sela, J. (1980) Spectral modeling at the National Meteorological Center, Mon. Wea. Rev. 108:1279-1292.

4. Eliasen, E., Machenauer, B., and Rasmussen, E. (1970) On a Numerical Method for Integration of the Hydrodynamical Equations With a Spectral Representation of the Horizontal Fields. Inst. of Theor. Meteorology, Univ. of Copenhagen, Report No. 2.

5. Orszag, S.A. (1970) Transform method for calculation of vector coupled sums: Application to the spectral form of the vorticity equation, J. Atmos. Sci. 27:890-895.

of the current state-of-the-art and with an eye towards the future it was decided that the AFGL global model should be similar to other multilayer spectral models - that is, horizontal variations represented by expansions in truncated series of spherical harmonics and vertical variations represented by values at discrete layers. The coarse resolution model (rhomboidal truncation at wavenumber 15 with six layers) described in this report establishes the baseline version for future comparisons. It closely follows the formulation of the current operational model at the National Meteorological Center (NMC).[3]

## 2. MODEL EQUATIONS

### 2.1 Continuous Equations

We begin with the equations of motion for an ideal gas in hydrostatic balance surrounding a rotating spherical planet. The coordinate system is the familiar $(\lambda, \phi, \sigma)$ system in which $\lambda, \phi$ are longitude and latitude, respectively, and

$$\sigma = \frac{p}{p_*}$$

is the terrain following coordinate suggested by Phillips,[6] where p is the pressure and $p_*$ is the surface value of p. The horizontal momentum equations are replaced by the equations for absolute vorticity and divergence

$$\eta = f + \zeta = f + \underset{\sim}{k} \cdot \nabla x \underset{\sim}{v}$$

$$D = \nabla \cdot \underset{\sim}{v}$$

where f is the coriolis parameter, $\underset{\sim}{v}$ is the horizontal wind vector, and $\underset{\sim}{k}$ is the vertical unit vector. These two equations are written in the form suggested by Bourke[7]

$$\frac{\partial \eta}{\partial t} = - \frac{1}{a \cos^2 \phi} \left[ \frac{\partial A}{\partial \lambda} + \cos \phi \frac{\partial B}{\partial \phi} \right] + \underset{\sim}{k} \cdot \nabla x \underset{\sim}{F}_h \qquad (1)$$

---

6. Phillips, N.A. (1957) A coordinate system having some special advantages for numerical forecasting, J. Meteorol. 14:184-185.
7. Bourke, W. (1974) A multi-level spectral model. I. Formulation and hemispheric integrations, Mon. Wea. Rev. 102:687-701.

$$\frac{\partial D}{\partial t} = \frac{1}{a \cos^2 \phi}\left[\frac{\partial B}{\partial \lambda} - \cos \phi \frac{\partial A}{\partial \phi}\right] - \nabla^2 [E + \Phi + RT_0 q] + \nabla \cdot \underset{\sim}{F}_h \quad , \tag{2}$$

where a is the radius of the earth, R is the gas constant for dry air, $\Phi$ is the geopotential height, $T_0$ is a fixed basic state temperature, which is a function of $\sigma$ only, and $\underset{\sim}{F}_h$ is the parameterized subgrid scale horizontal diffusion. Also, we have

$$A = \eta U + \dot{\sigma} \frac{\partial V}{\partial \sigma} + \frac{RT'}{a} \cos \phi \frac{\partial q}{\partial \phi} + \frac{g}{p_*} \frac{\partial \tau_\phi}{\partial \sigma} \tag{3}$$

$$B = \eta V - \dot{\sigma} \frac{\partial U}{\partial \sigma} - \frac{RT'}{a} \frac{\partial q}{\partial \lambda} - \frac{g}{p_*} \frac{\partial \tau_\lambda}{\partial \sigma} \tag{4}$$

$$E = \frac{U^2 + V^2}{2 \cos^2 \phi} \tag{5}$$

$$q = \ln p_* \quad , \tag{6}$$

where the pseudo-velocity components are $U = u \cos \phi$ and $V = v \cos \phi$, $\dot{\sigma}$ is the total derivative of $\sigma$ (that is, the vertical velocity), $T'$ is the deviation of temperature from the value $T_0$, and $\tau_\phi$, $\tau_\lambda$ are the components of the surface stress that are described in Section 3.1. The pseudo-velocity components are obtained from the following diagnostic relationships among vorticity, divergence, streamfunction, velocity potential, and horizontal velocity components

$$U = -\frac{\cos \phi}{a} \frac{\partial \psi}{\partial \phi} + \frac{1}{a} \frac{\partial \chi}{\partial \lambda} \tag{7}$$

$$V = \frac{1}{a} \frac{\partial \psi}{\partial \lambda} + \frac{\cos \phi}{a} \frac{\partial \chi}{\partial \phi} \tag{8}$$

$$\zeta = \nabla^2 \psi \tag{9}$$

$$D = \nabla^2 \chi \quad , \tag{10}$$

where $\psi$ is the streamfunction and $\chi$ is the velocity potential.

The continuity equation is

$$\frac{\partial q}{\partial t} = - C - D - \frac{\partial \dot{\sigma}}{\partial \sigma} \quad , \tag{11}$$

where $C = \underline{v} \cdot \nabla q$. Vertical integration of Eq. (11) with the boundary conditions $\dot{\sigma} = 0$ at $\sigma = 0$ and $\sigma = 1$ gives a prognostic for the surface pressure

$$\frac{\partial q}{\partial t} = - \bar{C} - \bar{D} \tag{12}$$

and a diagnostic for $\dot{\sigma}$

$$\dot{\sigma} = \sigma(\bar{C} + \bar{D}) - \bar{C}^{\sigma} - \bar{D}^{\sigma} \quad , \tag{13}$$

where

$$(\bar{\ })^{\sigma} = \int_0^{\sigma} (\ ) \, d\sigma \text{ and } (\bar{\ }) = \int_0^{1} (\ ) \, d\sigma \quad . \tag{14}$$

The hydrostatic and thermodynamic equations are written in the forms that are suited to the Arakawa vertical differencing scheme.[8, 1] The hydrostatic equation is

$$\frac{\partial \Phi}{\partial \sigma^{\kappa}} = - C_p T \sigma^{-\kappa} \quad , \tag{15}$$

where $C_p$ is the specific heat of dry air at constant pressure, $\kappa = R/C_p$, and the temperature is given by $T = T_0(\sigma) + T'$. The thermodynamic equation is

$$\frac{\partial T}{\partial t} = - \frac{1}{a \cos^2 \phi} \left[ \frac{\partial UT'}{\partial \lambda} + \cos \phi \, \frac{\partial VT'}{\partial \phi} \right] + T'D$$

$$- \sigma^{\kappa} \dot{\sigma} \, \frac{\partial T \sigma^{-\kappa}}{\partial \sigma} + \frac{RT}{C_p} [C - \bar{C} - \bar{D}] + \frac{H}{C_p} + {}_hF_T \quad , \tag{16}$$

8. Arakawa, A., and Mintz, Y. (1974) The UCLA Atmospheric Circulation Model, Dept. of Meteorology, University of California.

where H is the heating rate due to the diabatic effects of convection, condensation, evaporation, and turbulent heat transfer, and ${}_hF_T$ is the parameterized subgrid scale horizontal diffusion. All of these are included in the parameterized physical processes that are described in Section 3.

The forecast model is completed with a prognostic equation for specific humidity, Q,

$$\frac{\partial Q}{\partial t} = -\frac{1}{a\cos^2\phi}\left[\frac{\partial UQ}{\partial\lambda} + \cos\phi\,\frac{\partial VQ}{\partial\phi}\right] + QD - \dot{\sigma}\,\frac{\partial Q}{\partial\sigma} + S + {}_hF_Q \qquad (17)$$

where S is the rate of change of Q due to moist convection, condensation, and evaporation, and ${}_hF_Q$ is the parameterized subgrid scale horizontal diffusion. Once again these physical processes are described in Section 3.

### 2.2 Numerical Methods

Because of the complexity of the model equations, realistic solutions can be obtained only through numerical simulation. In this section we turn our attention to the system of finite mathematics that is used to solve the equations. For convenience, we consider the numerical methods in three parts: horizontal, vertical, and time.

#### 2.2.1 HORIZONTAL

In the horizontal domain, we assume that spatial variations can be represented by expanding each of the dependent variables in a truncated series of surface spherical harmonics, for example,

$$\eta(\lambda,\phi,\sigma,t) = \sum_{m=-M}^{M}\sum_{n=|m|}^{N}\eta_n^m(\sigma,t)Y_n^m(\lambda,\sin\phi) \quad , \qquad (18)$$

where $Y_n^m(\lambda,\sin\phi) = P_n^m(\sin\phi)\,e^{im\lambda}$ is the spherical harmonic of order m and degree n, $P_n^m(\sin\phi)$ is the normalized associated Legendre function of the first kind, and M and N are the truncation wavenumbers. The time- and $\sigma$-dependent spectral coefficients, $\eta_n^m$ etc., are complex and reality of the various fields requires $\eta_n^{-m} = (-1)^m(\eta_n^m)^*$ where $(\,)^*$ is the complex conjugate. The type of truncation (for example, rhomboidal or triangular) depends upon the choice of N. For the baseline model, we will use a rhomboidal truncation, $N = |m| + M$, with $M = 15$.

To obtain the equations in spectral form, expansions of the form Eq. (18) are substituted into the continuous equations, and then the equations are operated on by the transform operator

$$( )_n^m = \frac{1}{2\pi} \int_0^{2\pi} \int_{-\frac{\pi}{2}}^{\frac{\pi}{2}} ( ) P_n^m(\sin \phi) \cos \phi \, d\phi \, e^{-im\lambda} \, d\lambda \tag{19}$$

for all (m, n).

In the classical spectral method, it is necessary to evaluate the interaction coefficients (for example, Silberman[9]) in order to determine the spectral coefficients of the nonlinear terms in the prognostic equations. These are integrals over latitude of products of various combinations of three associated Legendre functions. Their evaluation on a computer is quite time and memory consuming. To avoid these computations, we use the transform method that was developed by Eliasen et al[4] and independently by Orszag.[5] In practice, the method consists of three distinct steps:

(a) transform the dependent variables from spectral space to physical grid space;

(b) perform the required nonlinear multiplications in grid space; and

(c) transform the nonlinear products from grid space to spectral space.

Transform steps (a) and (c) consist of a pair of transforms, a Legendre transform (spherical harmonic space to Fourier space and back), and a Fourier transform (Fourier space to grid space and back). For the inverse transform step (a) the Legendre transform is accomplished by actually summing the Legendre series, while the Fourier transform is computed with an inverse fast Fourier transform (FFT) algorithm. For the forward transform step (c), the Fourier transform is computed by the FFT while the integral of the Legendre transform is evaluated by a Gaussian quadrature. The Gaussian quadrature is exact for our integrands (that is, polynomials) given a sufficient number of points (Gaussian latitudes).[4] For rhomboidal truncation, the transform grid required to provide alias-free evaluation of quadratic nonlinear interactions consists of at least 3M + 1 equally-spaced longitudes and at least (5M + 1)/2 Gaussian latitudes. For our truncation of M = 15 we use 48 longitudes (7.5° spacing) and 40 Gaussian latitudes (~4.4° spacing).

9. Silberman, J.S. (1954) Planetary waves in the atmosphere, J. Meteorol. 11:27-34.

Finally, in presenting the spectral equations, we will use the following relationships

$$\frac{\partial Y_n^m}{\partial \lambda} = imY_n^m \tag{20}$$

$$-\cos\phi \frac{dP_n^m}{d\phi} = n\varepsilon_{n+1}^m P_{n+1}^m - (n+1)\varepsilon_n^m P_{n-1}^m \equiv H_n^m \tag{21}$$

$$\nabla^2 Y_n^m = \frac{-n(n+1)Y_n^m}{a^2} \quad , \tag{22}$$

where

$$\varepsilon_n^m = \left[\frac{n^2 - m^2}{4n^2 - 1}\right]^{1/2} \quad .$$

Following Bourke's[2] notation, the spectral prognostic equations are (excluding parameterized physics)

$$\frac{\partial \eta_n^m}{\partial t} = -L_n^m(A_m, B_m) \tag{23}$$

$$\frac{\partial D_n^m}{\partial t} = L_n^m(B_m, -A_m) + \frac{n(n+1)}{a^2}\left[E_n^m + \Phi_n^m + RT_0 q_n^m\right] \tag{24}$$

$$\frac{\partial T_n^m}{\partial t} = -L_n^m\left((UT')_m, (VT')_m\right) + I_n^m \tag{25}$$

$$\frac{\partial Q_n^m}{\partial t} = -L_n^m\left((UQ)_m, (VQ)_m\right) + J_n^m \tag{26}$$

$$\frac{\partial q_n^m}{\partial t} = -\tilde{C}_n^m - \tilde{D}_n^m \quad , \tag{27}$$

where

$$L_n^m(x_m, y_m) = \int_{-\frac{\pi}{2}}^{\frac{\pi}{2}} \frac{1}{a \cos^2 \phi} \left[ imx_m P_n^m + y_m H_n^m \right] \cos \phi \, d\phi \tag{28}$$

$$I = T'D - \sigma^{\kappa} \dot{\sigma} \frac{\partial T\sigma^{-\kappa}}{\partial \sigma} + \frac{RT}{C_p} (C - \bar{C} - \bar{D}) \tag{29}$$

$$J = QD - \dot{\sigma} \frac{\partial Q}{\partial \sigma} \quad . \tag{30}$$

A subscript m indicates a Fourier coefficient and the other nonlinear terms are defined above in Section 2.1. We note that the diabatic heating, H, and the moisture source/sink term, S, are not included in Eqs. (29) and (30), respectively, since these parameterized processes are treated as adjustment terms that are added at the end of each time-step.

The only diagnostic equation that is treated spectrally is the hydrostatic equation. Since it is a linear equation we can immediately write

$$\frac{\partial \Phi_n^m}{\partial \sigma^{\kappa}} = -C_p T_n^m \sigma^{-\kappa} \quad . \tag{31}$$

The equations for U and V could also be written in spectral form. However, U and V are only required in evaluating the nonlinear terms, and therefore we determine their Fourier coefficients directly from the harmonic coefficients of vorticity and divergence with the aid of the spectral equivalents of Eqs. (9) and (10):

$$U_m = -a \sum_{n=|m|}^{N} \frac{1}{n(n+1)} \left[ \zeta_n^m H_n^m + imD_n^m P_n^m \right] \tag{32}$$

$$V_m = -a \sum_{n=|m|}^{N} \frac{1}{n(n+1)} \left[ im\zeta_n^m P_n^m - D_n^m H_n^m \right] \quad . \tag{33}$$

We point out that because of the form of $H_n^m$, Eqs. (32) and (33) imply that a direct spherical harmonic representation in terms of $U_n^m$ and $V_n^m$ would require that one additional mode be retained for each m. Thus, the Legendre series for $U_m$ and $V_m$ (in terms of $U_n^m$, $V_n^m$) would be truncated at N + 1 instead of N.

Finally, we note that $\dot{\sigma}$ is not considered spectrally since it is needed only in grid space for computing the vertical advection terms in the nonlinear interactions.

### 2.2.2 VERTICAL STRUCTURE

In the vertical, the model is divided into a number of discrete layers. The interfaces between layers are referred to as levels and thus the number of levels is one more than the number of layers. All of the dependent variables (prognostic and diagnostic) except $\dot{\sigma}$ are considered as layer variables. The values of $\dot{\sigma}$ are carried at the levels. Typical layering and variable locations are illustrated in Figure 1 (note: a tilde ($\sim$) indicates a quantity that is evaluated at the levels). The current version of the model includes six layers and seven levels with $\sigma$ and $\tilde{\sigma}$ locations and layer thickness, $\Delta$, according to the values in Table 1. This structure was established by defining four equally-spaced $\sigma$ layers and then dividing the lowest and uppermost layers into two layers each. This is done to provide additional resolution of the planetary boundary layer and the tropopause region. Since the structure is set by specifying the number of layers and their spacing, the

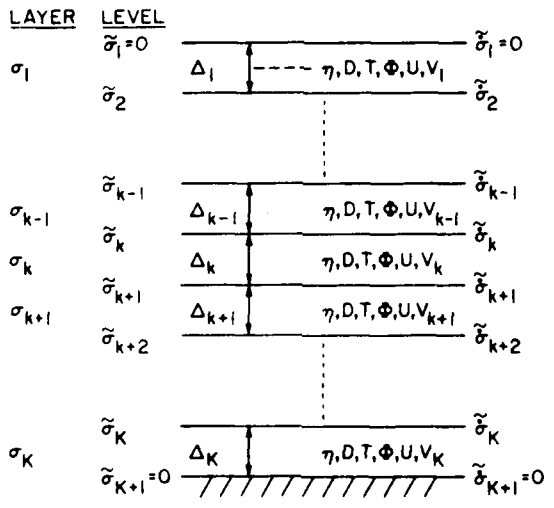


Figure 1. Vertical Layering and Variable Location

Table 1. Current Vertical Structure

| Level | $\tilde{\sigma}$ | $\sigma$ | Layer | $\Delta$ |
|---|---|---|---|---|
| 1 | 0 | | | |
| | | 0.0622 | 1 | 0.15 |
| 2 | 0.15 | | | |
| | | 0.1985 | 2 | 0.10 |
| 3 | 0.25 | | | |
| | | 0.3699 | 3 | 0.25 |
| 4 | 0.50 | | | |
| | | 0.6220 | 4 | 0.25 |
| 5 | 0.75 | | | |
| | | 0.8242 | 5 | 0.15 |
| 6 | 0.90 | | | |
| | | 0.9497 | 6 | 0.10 |
| 7 | 1.00 | | | |

values of $\tilde{\sigma}$ at the levels are immediately prescribed. Determining the values of $\sigma$ in the layers (that is, the point at which the dependent variables should be located) is not so straightforward. Many researchers have chosen to simply pick the midpoint of each layer (for example, Bourke[7]). However, since we have chosen to construct our baseline model according to the NMC formulation, we follow Sela[3] and determine $\sigma$ in the layers from

$$\sigma_k^{\kappa} = \frac{\tilde{\sigma}_{k+1}^{1+\kappa} - \tilde{\sigma}_k^{1+\kappa}}{(1+\kappa)(\tilde{\sigma}_{k+1} - \tilde{\sigma}_k)} \approx \frac{1}{1+\kappa} \frac{d\sigma^{1+\kappa}}{d\sigma} \quad . \tag{34}$$

In order to evaluate vertical advection terms, they are first rewritten in flux form, for example,

$$\dot{\sigma} \frac{\partial U}{\partial \sigma} = \frac{\partial \dot{\sigma} U}{\partial \sigma} - U \frac{\partial \dot{\sigma}}{\partial \sigma} \quad , \tag{35}$$

The finite difference analog of the flux form for layer k is

$$\frac{\partial \dot{\sigma} U}{\partial \sigma} - U \frac{\partial \dot{\sigma}}{\partial \sigma} \approx \frac{\tilde{\dot{\sigma}}_{k+1} \tilde{U}_{k+1} - \tilde{\dot{\sigma}}_k \tilde{U}_k}{\Delta_k} - U_k \frac{\tilde{\dot{\sigma}}_{k+1} - \tilde{\dot{\sigma}}_k}{\Delta_k} \quad . \tag{36}$$

Since U is a layer variable, we must interpolate the layer values to determine $\tilde{U}$ (that is, the level values). Following Arakawa[8] we use the relationship

$$\tilde{U}_{k+1} = \frac{1}{2} (U_{k+1} + U_k) \tag{37}$$

and upon substituting into Eq. (36) we have

$$\frac{\partial \dot{\sigma} U}{\partial \sigma} - U \frac{\partial \dot{\sigma}}{\partial \sigma} \approx \frac{1}{2\Delta_k} \left[ \tilde{\dot{\sigma}}_{k+1} (U_{k+1} - U_k) + \tilde{\dot{\sigma}}_k (U_k - U_{k-1}) \right] \quad , \tag{38}$$

which is a quadratic conserving differencing scheme. Similar expressions can be written for vertical advection terms involving V and Q.

For the vertical advection term in the thermodynamic equation, Eq. (29), and for the hydrostatic equation, Eq. (31), we apply Eq. (37) to the entire quantity $T\sigma^{-\kappa}$ so that $\tilde{T}$ is determined from

$$\tilde{T}_{k+1} = \frac{\tilde{\sigma}^{\kappa}_{k+1}}{2} \left( \frac{T_{k+1}}{\sigma^{\kappa}_{k+1}} + \frac{T_k}{\sigma^{\kappa}_k} \right) \quad . \tag{39}$$

Thus, the vertical advection term in the thermodynamic equation (in flux form) is given by

$$\sigma^{\kappa} \frac{\partial \dot{\sigma} T \sigma^{-\kappa}}{\partial \sigma} - T \frac{\partial \dot{\sigma}}{\partial \sigma} \approx \frac{1}{2\Delta_k} \left[ \tilde{\dot{\sigma}}_{k+1} \left( \frac{\sigma^{\kappa}_k}{\sigma^{\kappa}_{k+1}} T_{k+1} - T_k \right) + \tilde{\dot{\sigma}}_k \left( T_k - \frac{\sigma^{\kappa}_k}{\sigma^{\kappa}_{k+1}} T_{k-1} \right) \right] \quad . \tag{40}$$

The finite difference analogs of the vertical integrals of Eq. (14) are

$$(\bar{\ })^{\tilde{\sigma}_{k+1}} = \int_0^{\tilde{\sigma}_{k+1}} (\ ) \, d\sigma \approx \sum_{j=1}^{k} (\ )_j \, \Delta_j \tag{41}$$

and

$$(\bar{\ }) = \int_0^1 (\ )\, d\sigma \approx \sum_{j=1}^{K} (\ )_j \Delta_j \quad . \tag{42}$$

We conclude this subsection by considering the solution of the hydrostatic equation. With the aid of Eq. (39), the finite difference form of the hydrostatic equation is

$$\Phi_k - \Phi_{k+1} = \alpha_{k+1} T_{k+1} + \beta_k T_k \quad , \tag{43}$$

where

$$\alpha_{k+1} = \frac{C_p}{2} \left( 1 - \frac{\sigma_k^\kappa}{\sigma_{k+1}^\kappa} \right)$$

and

$$\beta_k = \frac{C_p}{2} \left( \frac{\sigma_{k+1}^\kappa}{\sigma_k^\kappa} - 1 \right) \quad .$$

The geopotential of the lowest layer is determined from the integral constraint

$$\int_0^1 [RT - (\Phi - \Phi_*)]\, d\sigma = 0 \quad , \tag{44}$$

where $\Phi_*$ is the surface geopotential (that is, terrain height). In finite difference form Eq. (44) is

$$\sum_{k=1}^{K} [RT_k - (\Phi_k - \Phi_*)] \Delta_k = 0 \quad . \tag{45}$$

Upon combining Eqs. (43) and (45) we have an expression for the height of the lowest layer, $\Phi_K$

$$\Phi_K - \Phi_s = RT_K\Delta_K + \sum_{k-1}^{K-1}\left[RT_k - \sum_{j=k}^{K-1}(\alpha_{j+1}T_{j+1} + \beta_j T_j)\right]\Delta_k \quad . \tag{46}$$

Thus, the geopotential for all layers can be determined from the hydrostatic equation by solving Eq. (46) for the lowest layer followed by Eq. (43) for all other layers.

2.2.3 TIME INTEGRATION

The time integration is accomplished by the so-called semi-implicit method, which is a mixture of implicit and explicit techniques. In this method, linear terms associated with gravity waves in the time-dependent equations are treated implicitly while other terms are treated explicitly. Such an approach avoids the problem of having to deal with a nonlinear algebraic system associated with implicit methods for nonlinear differential equations; and yet it gives us a time integration scheme in which relatively large time increments can be used (Robert[10]). Had we used an explicit scheme, computational stability considerations would have dictated the use of a much smaller time increment (for example, 10 min for a leap frog scheme as compared to 60 min for the semi-implicit scheme).

There are various ways to implement the semi-implicit method. The one adopted here is due to Bourke.[7] The key point is to eliminate T and q among the discrete forms of Eqs. (24), (25), and (27), leaving D as the sole unknown. The mathematical details of the derivation of the algebraic divergence equation are given in Appendix B. Here we only outline the procedure:

(a) Express $\Phi$ in Eq. (24) in terms of T, using the hydrostatic equations, Eqs. (43) and (46) and

(b) Approximate time derivatives in Eqs. (23) through (27) by

$$\frac{\partial F}{\partial t} = \frac{F^+ - F^-}{2\Delta t} \quad .$$

Here F is any of the prognostic variables, and $F^+$ and $F^-$ are values of the variables at the next and previous time-steps, respectively.

(c) Replace F in the linear terms on the right-hand side of Eqs. (24), (25), and (27) by

---

10. Robert, A. (1979) The semi-implicit method, Numerical Methods Used in Atmospheric Models, Vol. 2. GARP Publication Series, No. 17. Geneva, WMO, pp. 419-430.

$$F = \alpha F^{+} + (1 - \alpha) F^{-} \quad ,$$

where $1/2 \leq \alpha \leq 1$,

(d) Eliminate $T^{+}$, $q^{+}$ in the discrete divergence equation by using the discrete forms of Eqs. (25) and (27), thus leaving an algebraic system in $D^{+}$. Once $D^{+}$ values are found, Eqs. (25) and (27) can immediately be solved for $T^{+}$ and $q^{+}$. Since there are no linear terms on the right-hand side of the vorticity and moisture equations, these two equations are integrated explicitly.

In the current version of our model, the following time-stepping sequence has been implemented:

(a) Advance $\eta$ and Q using an explicit leap frog scheme,

(b) Advance D to the new time step $t + \Delta t$ by solving the linear algebraic system Eq. (B11) from Appendix B,

(c) Advance T and q using Eqs. (B9) and (B10) from Appendix B,

(d) Apply the moisture physics and adjust the predicted values of T and Q, and

(e) Time-smooth all of the prognostic variables at current time t to prevent decoupling between the even and odd time-step values. Thus, the latest predicted value of a variable, $F^{+}$, is used to compute a time-smoothed value for the next time-stepping cycle:

$$F^{*} = F + \beta(F^{-} - 2F + F^{+}) \quad ,$$

where $F^{*}$ becomes the time-smoothed $F^{-}$ value for the next time-cycle, and $\beta$ is a given constant. For the very first time-step, a forward scheme is used.

For the results reported below we use the values $\Delta t = 60$ min, $\alpha = 1$ (backward implicit), and $\beta = 0.02$.

## 3. PARAMETERIZED PHYSICAL PROCESSES

To establish our baseline model, we have adapted the various parameterized physical processes that appear in the current NMC spectral model.[3] These fall into three broad categories: boundary layer processes; moisture physics, including convective adjustment as well as the so-called large-scale saturation process; and subgrid scale diffusion.

### 3.1 Boundary Layer Physics

Boundary layer processes are included in the model to simulate the interaction between the surface of the earth and the atmosphere. In particular, three

mechanisms are considered in terms of fluxes into the atmosphere: surface friction (that is, momentum flux), sensible heat flux from the surface, and evaporation from the surface (that is, moisture flux).

The surface friction is formulated following Bourke[7] with some minor modifications. It is simulated by including the stress terms

$$\frac{g}{p_*}\frac{\partial \tau_\phi}{\partial \sigma} \quad \text{and} \quad \frac{-g}{p_*}\frac{\partial \tau_\lambda}{\partial \sigma} \tag{47}$$

in Eqs. (3) and (4), respectively. For purposes of the vertical finite difference scheme, $\tau_\lambda$ and $\tau_\phi$ are defined at the levels and are set to zero except at the surface where they are given by the bulk aerodynamic formula

$$\underset{\sim}{\tau}_* = \rho C_d \sqrt{2E}\, \underset{\sim}{V}_* \quad ,$$

where $\rho$ is the density, $C_d$ is the drag coefficient, E is the kinetic energy, and $\underset{\sim}{V}_*$ is the horizontal vector whose components are the pseudo-velocities U, V at the surface of the earth. Strictly speaking, $\rho$ and E should also be evaluated at the surface. However, in view of the crude nature of the stress formulation and for simplicity, $\rho$ and E are assigned the values from the lowest model layer. $\underset{\sim}{V}_*$ is given by $\underset{\sim}{V}$ at the lowest layer rotated by an amount $\alpha$ towards low pressure. In addition, a latitudinal weighting factor of $\sin\phi$ is included with $\sin\alpha$ to reduce the influence of turning near the equator and to provide the proper sense of rotation in the Southern Hemisphere. Thus, the surface stress terms are given by

$$(\tau_*)_\lambda = \rho_K C_d \sqrt{2E_K}\,(U_K \cos\alpha - V_K \sin\alpha \sin\phi)$$

$$(\tau_*)_\phi = \rho_K C_d \sqrt{2E_K}\,(V_K \cos\alpha + U_K \sin\alpha \sin\phi) \quad , \tag{49}$$

where a subscript K indicates the value at the lowest model layer. The value of $\alpha = 20^\circ$ is fixed for all locations. Values of $C_d$ vary geographically from a minimum of 0.0013 over the open oceans to a maximum of 0.009 over the Himalayas.

Sensible heat transfer from the surface is included as part of the diabatic heating term, $\frac{H}{C_p}$, in the thermodynamic Eq. (16). The parameterization allows only an upward heat flux into the lowest model layer and only over the oceans. The exact form of the heating term is

$$\frac{H}{C_p} = \frac{g}{p_*}\frac{\partial F_\theta}{\partial \sigma} \quad , \tag{50}$$

where $F_\theta$ is defined at the levels and is set to zero except at the surface where it is given by the bulk aerodynamic formula

$$(F_\theta)_* = \rho_K C_T \sqrt{2E_K} (\theta_* - \theta_K) \quad , \tag{51}$$

where $\theta$ is the potential temperature, a subscript K indicates the value at the lowest model layer, and $C_T$ is the thermal drag coefficient given by

$$C_T = C_d + 7 \times 10^{-5} \sqrt{2E_K} \quad . \tag{52}$$

This formulation of $C_T$ allows the heat transfer process to be highly wind-speed selective (that is, it becomes more efficient as the wind speed increases). For these computations we use $p_*$ as the reference pressure for defining potential temperature and thus Eq. (51) becomes

$$(F_\theta)_* = \rho_K C_T \sqrt{2E_K} (T_* - T_K \sigma_K^{-\kappa}) \quad , \tag{53}$$

where $T_*$ is the sea surface temperature.

Evaporation from the surface is included in the moisture source/sink term, S, in Eq. (17). Evaporation is allowed only over the oceans and only if the lowest model layer is not saturated relative to the ocean surface and/or there is no precipitation in the lowest layer. The mathematical formulation of the evaporation physics closely resembles the sensible heat transfer. The form of the evaporation term is

$$S = \frac{g}{p_*} \frac{\partial F_Q}{\partial \sigma} \tag{54}$$

where $F_Q$ is defined at the levels and is set to zero except at the surface where it is given by

$$(F_Q)_* = \rho_K C_Q \sqrt{2E_K} (Q_s(T_*) - Q_K) \quad , \tag{55}$$

where $Q_s(T_*)$ is the saturation specific humidity at the sea surface temperature, and the moisture drag coefficient is given by

$$C_Q = C_T = C_d + 7 \times 10^{-5} \sqrt{2E_K} \quad . \tag{56}$$

Finally, to provide additional computational stability, the surface drag, the heat flux, and the moisture flux are lagged in time.

### 3.2 Moisture Physics

In this section we describe the parameterization of the processes that are associated with the phase changes of water. These are adapted directly from the NMC spectral model[3] with only minor modifications to account for the difference between the sigma structures of the two models. The values of pressure-dependent parameters that appear in the algorithms are defined by simple interpolations of those employed by NMC. The procedure consists of a sequence of three adjustments of temperature and specific humidity. Each step represents a particular aspect of physics involving the vertical stratification of the variables. The adjustments are applied after the provisional values of the dynamic variables at a new time step are obtained through time integration.

The current practice makes no distinction between liquid and solid phases and all values of the relevant physical parameters such as specific heat and latent heat refer only to either gaseous or liquid state.

#### 3.2.1 CONVECTIVE ADJUSTMENT

The first adjustment is based on Kuo's[11] simulation of organized cumulus convection. This moist convective adjustment scheme consists of two parts. The first part of the scheme, which has been described in great detail by Phillips,[12] accounts for the changes that occur in temperature and specific humidity when convection redistributes heat and moisture in a moist unstable column. In implementing the scheme, the only change we make in Phillips' description is the critical value of the moisture convergence above which the adjustment is invoked. We use a value of $1 \times 10^{-7} \cdot \Delta t$ cb $s^{-1}$ where $\Delta t$ is the time step in seconds. This is the appropriate value for our choice of vertical structure.

The second part of the convective adjustment scheme takes into account the effects of evaporation of falling water. This will cause changes in temperature, specific humidity, and the amount of rainfall. Phillips only gives a brief description of this part and thus, for the sake of completeness, we provide the balance.

First, we define the moisture deficit for each unsaturated layer in the unstable column

---

11. Kuo, H. L. (1965) On formation and intensification of tropical cyclones through latent heat release by cumulus convection, J. Atmos. Sci. 22:40-63.

12. Phillips, N. A. (1979) The Nested Grid Model, NOAA Technical Report NWS-22, 79 pp.

$$Q_{def,k} = (Q^{*}_{sat,k} - Q_{0,k})\Delta\sigma_k \quad , \tag{57}$$

where $Q^{*}_{sat,k}$ is the effective saturation specific humidity (chosen to be eight-tenths of the theoretical value), $Q_{0,k}$ is the latest provisional value of specific humidity, and $\Delta\sigma_k$ is the thickness of the layer.

The amount of total condensate, F, starts in the highest saturated layer of the unstable column with the value given by

$$F_k = \frac{C_p}{L_v} DTKUO_k \Delta\sigma_k \quad , \tag{58}$$

in which DTKUO denotes the temperature adjustment to that layer brought about by the Kuo convection. As the condensate falls it will either undergo evaporation in unsaturated layers or accumulate additional condensate in saturated layers.

In an unsaturated layer, evaporation must continue until all of the condensate evaporates or until the layer becomes saturated. In the former case $Q_{def,k} > F_k$, and the adjusted values of specific humidity, temperature, and condensate are

$$Q_{1,k} = Q_{0,k} + F_{k-1}/\Delta\sigma_k$$

$$T_{1,k} = T_{0,k} - \frac{C_p}{L_v} \frac{F_{k-1}}{\Delta\sigma_k}$$

$$F_k = 0 \quad . \tag{59}$$

In the later case $Q_{def,k} < F_k$, and only a part of condensate evaporates, thus bringing the layer to the level of effective saturation, with the results

$$Q_{1,k} = Q^{*}_{sat,k}$$

$$T_{1,k} = T_{0,k} - \frac{C_p}{L_v} Q_{def,k}$$

and

$$F_k = F_{k-1} - \frac{Q_{def,k}}{\Delta\sigma_k} \quad . \tag{60}$$

In a saturated layer, Q and T remain unchanged and F accumulates the additional condensate so that

$$F_k = F_{k-1} + \frac{c_p}{L_v} DTKUO_k \, \Delta\sigma_k \quad . \tag{61}$$

Finally, the amount of rainfall, G, is given by

$$G = F_K \frac{p_s}{g} \tag{62}$$

where $p_s$ is the surface pressure.

3.2.2 LARGE-SCALE SATURATION

The second adjustment, which is also described in Phillips' report, is referred to as the large-scale saturation process. It is purported to adjust temperature and specific humidity according to the wet-bulb relation. There is, however, built-in empiricism in the formulas currently used to calculate the amounts of assumed and allowable evaporations. A brief account of these aspects is given here.

For each layer we define

$$\begin{aligned} Q_{app,k} &= C_{app} Q_{s,k} \\ Q_{eff,k} &= C_{eff} Q'_{s,k} \quad , \end{aligned} \tag{63}$$

where $Q_{app}$ and $Q_{eff}$ will be referred to as the apparent saturation specific humidity and the effective saturation specific humidity, respectively. $C_{app}$ and $C_{eff}$ are empirical constants that are determined as follows. $C_{app}$ takes the value of 0.95 in the topmost of the moisture-carrying layers and 0.80 elsewhere. On the other hand, $C_{eff}$ assumes the value of unity in the bottom layer and the value 0.85 in the fourth lowest layer and above. In the second and third lowest layers, however, it is assumed that $C_{eff}$ increases with temperature quadratically to the extent that its value lies in the range between 0.85 and 0.95. The relationship between $C_{eff}$ and temperature is given by

$$C_{eff} = 0.85 + x(1 + x)/200 \quad \text{if} \quad C_{eff} \leq 0.95 \quad , \tag{64}$$

where

$$x = \frac{T - 261.16}{8} \quad .$$

Next, in each of the moisture-carrying layers, a deficit, $S_k$, is defined by

$$S_k = \frac{p_*}{g} (Q_{0,k} - Q_{eff,k}) \Delta\sigma_k \quad , \tag{65}$$

where $Q_{0,k}$ is the latest provisional value of specific humidity. It is assumed that if $S_k < 0$ evaporation will occur and no additional precipitation is contributed by the layer. The amount of evaporation is given by

$$E = C \frac{p_*}{g} (Q_{0,k} - Q_{app,k}) \Delta\sigma_k \quad , \tag{66}$$

in which C is an efficiency factor ($0 < C < 1$) that decreases downward. The amount of precipitation reaching the adjacent layer below is then reduced by the amount E. If $S_k \geq 0$, on the other hand, there is no evaporation but an additional amount of precipitation represented by $S_k$ is contributed by the layer

Finally, the adjustments on temperature and specific humidity are given respectively by

$$Q_{1,k} = Q_{0,k} - \frac{g}{p_*} S_k$$

$$T_{1,k} = T_{0,k} + \frac{g}{p_*} \frac{L_v}{C_p} S_k \quad . \tag{67}$$

### 3.2.3 ADIABATIC ADJUSTMENT

The third adjustment insures that the thermal stratification is statically stable. When instability results from the last provisional values of temperature, it is assumed that complete mixing takes place in both heat and moisture so that the adjusted potential temperature and specific humidity assume uniform values that are the mass-weighted averages of the respective quantities within the unstable layer.

In addition to these adjustments that are based on physical reasoning, there are two other adjustments made on specific humidity that owe their existence to the computational aspects of the model. When the initial grid-point values of

specific humidity are transformed into spectral amplitudes, the latter are uniformly reduced to nine-tenths of the original values. The other adjustment is introduced when the spectral coefficients are transformed into grid-point values at each time step. Here, whenever a grid-point value turns out to be negative it is simply set to zero.

### 3.3 Subgrid Scale Diffusion

The parameterized subgrid scale diffusion in the model serves two purposes, both related to dissipative effects. From the point of view of physics, this process is included to simulate the assumed dissipative effect of the unresolved scales of motion. For computational purposes, it is included to prevent the spurious accumulation of energy in the smallest resolved scales of a numerical model with a finite spatial resolution.

In the current model, the diffusion is parameterized by adding a term of the form $-\nu\nabla^4(\ )$ to the prognostic equations for $\eta$, D, T, and Q. The $\nabla^4$ operator is more scale selective and more effective in controlling the higher wave numbers than the traditional $\nabla^2$ formulation. In practice, two different diffusion coefficients are used: $\nu_D = 4 \times 10^{17}\ m^4\ sec^{-1}$ for diffusion applied to all modes of the divergence, and $\nu_E = 1 \times 10^{16}\ m^4\ sec^{-1}$ for diffusion applied only to the upper half of the rhomboid ($n > M$) for $\eta$, T, and Q. For computational stability, the diffusion is lagged in time. There is no vertical diffusion included in the present formulation.

## 4. DATA PROCESSING

Before the model forecast can begin, the initial data must be prepared in a form appropriate for input into the model. Similarly, at the end of a forecast, the forecasted data must be put into a form appropriate for certain standard graphical and numerical displays.

In general, preparation of the initial data consists of three steps: (a) objective analysis in which the observed meteorological data are analyzed and represented at the mandatory pressure levels on a regular latitude-longitude grid; (b) preprocessing in which the analyzed data are transformed from the analysis grid at the mandatory pressure levels to the model grid in the model $\sigma$ layers and then transformed into spectral coefficients in the $\sigma$ layers; and (c) initialization in which the preprocessed data are put through a filtering procedure in which certain undesirable gravity modes (that is, meteorological noise) and their tendencies are removed. For the current baseline model we use the FGGE level III-A data that have already been analyzed; and thus we skip step (a). The preprocessing and the

normal-mode initialization have been adapted from the NMC spectral model.[3] The only changes made in these algorithms are those necessary to reflect the differences in resolution and $\sigma$ structure between the two models.

The postprocessing of the forecast data is essentially the inverse of the preprocessing, that is, the forecasted spectral coefficients in the model $\sigma$ layers are transformed to physical values at the mandatory pressure levels on a regular latitude-longitude grid. This procedure is also adapted from NMC.[3]

### 4.1 Preprocessing/Postprocessing

Since the preprocessing and postprocessing are essentially the inverse of one another, there are certain features that are common to both. The most prominent among them are the following:

(a) Between two levels $Z_a$ and $Z_b$ at which data are available, temperature, wind, and specific humidity are assumed to be piece-wise linear functions of $Z = \ln p$, that is,

$$F(Z) = F(Z_a) + A(Z - Z_a) \quad , \quad Z_a \leqq Z \leqq Z_b \quad , \tag{68}$$

where

$$A = \frac{F(Z_b) - F(Z_a)}{Z_b - Z_a} \quad .$$

(b) Geopotential and temperature are related to each other by the hydrostatic equation

$$\frac{\partial \Phi}{\partial Z} = -RT \quad . \tag{69}$$

It then follows from (a) that $\Phi$ is a piece-wise quadratic function of ln p and may be expressed as

$$\Phi(Z) = \Phi(\bar{Z}) + A(Z - \bar{Z}) + \frac{B}{2}(Z - \bar{Z})^2 \quad , \quad Z_a \leqq Z \leqq Z_b \quad , \tag{70}$$

where the constants A and B are determined from the observed values $\Phi(Z_a)$, $\Phi(Z_b)$, $T(Z_a)$, and $T(Z_b)$ by the following relations:

$$A = \frac{\Phi(Z_b) - \Phi(Z_a)}{Z_b - Z_a}$$

$$B = -R \frac{T(Z_b) - T(Z_a)}{Z_b - Z_a}$$

$$\bar{Z} = \frac{1}{2}(Z_a + Z_b) \quad . \tag{71}$$

### 4.1.1 PREPROCESSING

The first step of the preprocessing consists of transforming the analyzed data from the analysis grid to the model's computational grid. The FGGE level III-A data are available on a regular latitude-longitude grid with a spacing of $2.5^{\circ}$ (that is, 144 longitudes by 73 latitudes). The model grid consists of 48 equally-spaced longitudes ($7.5^{\circ}$ spacing) and 40 Gaussian latitudes ($\sim 4.4^{\circ}$ spacing). Thus for the longitudinal transformation we simply use every third data point. For the meridional transformation we use a two-point linear interpolation in $\mu = \sin\phi$.

The second, and more involved, step of the preprocessing consists of interpolating the data from the 12 mandatory pressure levels to the model's $\sigma$ layers. The analyzed data include geopotential, temperature, wind, and relative humidity at all pressure levels as well as geopotential at the surface of the earth. The required preprocessed data must consist of temperature, wind, and specific humidity for all $\sigma$ layers as well as pressure at the surface of the earth.

We begin by defining the model's $\sigma$-structure (see discussion in Section 2.2.2). Note that since $\sigma$ is an independent variable, $\sigma_k$ can be defined solely as a function of $\tilde{\sigma}_k$ and $\tilde{\sigma}_{k+1}$, the prescribed $\sigma$ values at the bounding surfaces of layer k. On the other hand, $p_k$, the pressure for layer k, is a dependent variable, and is given by

$$p_k(\lambda,\phi,t) = p_s(\lambda,\phi,t)\,\sigma_k \quad . \tag{72}$$

In order to determine $p_k(\lambda,\phi,t)$ we must first have $p_s(\lambda,\phi,t)$. For the remainder of this section, we shall omit any reference to $(\lambda,\phi,t)$ in the interest of brevity.

We determine $p_s$ by applying Eq. (70) at the earth's surface, that is, let $Z_s = \ln p_s$ and write Eq. (70) as

$$\frac{1}{2}B(Z_s - \bar{Z})^2 + A(Z_s - \bar{Z}) + \Phi(\bar{Z}) - \Phi_s = 0 \quad , \tag{73}$$

where A, B, and $\bar{Z}$ are given by Eq. (71) and

$$\Phi(\bar{Z}) = (\Phi_a + \Phi_b)/2 - B(Z_* - \bar{Z})^2/8 \quad . \tag{74}$$

Here the subscripts a and b indicate values at the two mandatory pressures that are nearest to the earth's surface. We can now easily solve Eq. (73), which is a quadratic equation for $Z_*$. Of the two solutions, however, only one is physically consistent. Once $Z_*$ is known, $p_*$, $p_k = p_* \sigma_k$ and $\tilde{p}_k = p_* \tilde{\sigma}_k$ may then be computed. With $\sigma_k$ defined and $p_*$ estimated, we may now proceed to compute layer values for the model variables.

As mentioned earlier, layer values for the model variables are computed by interpolating from the analyzed values at the mandatory pressures. To do this, geopotential values at model levels, $\tilde{p}_k$, are first computed by applying Eq. (70) at $\tilde{Z}_k = \ln \tilde{p}_k$:

$$\tilde{\Phi}_k = \Phi(\bar{Z}) + A(\tilde{Z}_k - \bar{Z}) + \frac{1}{2} B(\tilde{Z}_k - \bar{Z})^2 \qquad k = 1, K \quad , \tag{75}$$

where $\Phi(\bar{Z}) = (\Phi_a + \Phi_b)/2 - B(\tilde{Z}_k - \bar{Z})^2/8$, and B, A, and Z are given by Eq. (71). Here the subscripts a and b indicate values at the two adjacent mandatory pressures surrounding $\tilde{p}_k$. Next, layer temperatures $T_k$ are computed via the centered-difference form of Eq. (69)

$$T_{k-1} = -\frac{1}{R} \frac{\tilde{\Phi}_k - \tilde{\Phi}_{k-1}}{\tilde{Z}_k - \tilde{Z}_{k-1}} \qquad k = 2, K+1 \quad , \tag{76}$$

where $\tilde{\Phi}_{K+1} = \Phi_*$. With $T_k$ known, layer geopotential, $\Phi_k$, are obtained by solving the finite-difference hydrostatic Eqs. (46) and (43).

Layer values for the two components of the pseudo-velocity, $U_k = u_k \cos \phi$ $V_k = v_k \cos \phi$, and specific humidity $Q_k$ are computed by linear interpolation in Z. The appropriate relationship is Eq. (68) where F represents any one of the variables U, V, or Q.

Since analyzed moisture content is given in terms of relative humidity, RH, we must convert RH to Q before the vertical interpolation. For completeness, the conversion formulas are included here:

$$Q = \frac{0.622\, e}{p - 0.378\, e} \quad , \tag{77}$$

where

$$e = e_s \times RH \text{ cb}$$

$$e_s = b \exp(-a/T) \text{ cb}$$

$$a = \frac{\varepsilon L_v}{R} = \frac{2.51 \times 10^4}{1.61 \times 2.87} \ ^oK$$

$$b = e_s(273.16) \exp(a/273.16) = 0.611 \exp(a/273.16) \text{ cb} \quad .$$

The preprocessing is completed by transforming the variables from model grid values to a set of truncated spherical harmonic coefficients according to the forward transform procedure described in Section 2.2.1. The only additional point to note here is that the spherical harmonic coefficients of vorticity and divergence, $\eta_n^m$ and $D_n^m$, are computed spectrally from the Fourier coefficients of the pseudo-velocity components. This is done as follows: the definitions of vorticity and divergence are

$$\eta = \zeta + f = \frac{1}{a \cos^2 \phi}\left[\frac{\partial V}{\partial \lambda} - \cos\phi \frac{\partial U}{\partial \phi}\right] + 2\Omega \sin\phi$$

$$D = \frac{1}{a \cos^2 \phi}\left[\frac{\partial U}{\partial \lambda} + \cos\phi \frac{\partial V}{\partial \phi}\right] \tag{78}$$

and since these equations are linear, their Fourier transforms are simply

$$\eta_m = \frac{1}{a \cos^2 \phi}\left[imV - \cos\phi \frac{\partial U_m}{\partial \phi}\right] + \begin{cases} 2\Omega \sin\phi & m = 0 \\ 0 & m \neq 0 \end{cases}$$

$$D_m = \frac{1}{a \cos^2 \phi}\left[imU + \cos\phi \frac{\partial V_m}{\partial \phi}\right] . \tag{79}$$

The spherical harmonic coefficients can be obtained by applying the operator

$$\int_{-\pi/2}^{\pi/2} (\ )_m P_n^m \cos\phi \, d\phi$$

to Eq. (79). Noting the similarity in structure between Eq. (79) and the horizontal advection terms in the equations of motion (see Section 2) we find that $\eta_n^m$ and $D_n^m$ can be obtained by use of the operator $L_n^m$ defined in Eq. (28), that is,

$$\eta_n^m = L_n^m(V_m, -U_m) + \begin{cases} \sqrt{\frac{8}{3}}\,\Omega & (m,n) = (0,1) \\ 0 & (m,n) \neq (0,1) \end{cases}$$

$$D_n^m = L_n^m(U_m, V_m) \quad . \tag{80}$$

### 4.1.2 POSTPROCESSING

The problem of postprocessing is essentially the inverse of that of preprocessing. Here the spherical harmonic coefficients of geopotential and pressure at the earth's surface, and layer values of temperature, wind, and specific humidity are known. The problem is to find their values as well as those of the geopotential at mandatory levels on a latitude-longitude grid. Briefly, the procedure is as follows.

First, the grid point values of the variables on the $\sigma$ layers are computed from the spectral coefficients by using the inverse transform procedure described in Section 2.2.1. This can be done for any latitude-longitude grid. In this case, we use the analysis grid, that is, a regular spacing of $2.5^{\circ}$ in both latitude and longitude.

Next we must interpolate from the $\sigma$ layers back to the mandatory pressure surfaces. To find the geopotential at the mandatory pressures, we follow a three-step procedure:

(a) $\widetilde{\Phi}_k$ are computed from $T_k$ using the discrete hydrostatic equation

$$\widetilde{\Phi}_{k-1} = \widetilde{\Phi}_k - R\,T_{k-1}(\widetilde{Z}_{k-1} - \widetilde{Z}_k) \qquad k = K+1, \ldots, 2 \quad , \tag{81}$$

where

$$\widetilde{Z}_k = \ln \widetilde{p}_k = \ln (p_* \widetilde{\sigma}_k)$$

$$\widetilde{\Phi}_{K+1} = \Phi_*$$

$$\widetilde{p}_{K+1} = p_* \quad ,$$

(b) As a consequence of the hydrostatic approximation and the assumption that the geopotential is piece-wise quadratic in $Z$, $\widetilde{T}_k$ is now given by

$$\tilde{T}_k = (T_{k-1} + T_k)/2 + \frac{T_k - T_{k-1}}{Z_k - Z_{k-1}} \left( Z_k - \frac{Z_{k-1} + Z_k}{2} \right) \qquad k = 2, K \quad . \tag{82}$$

Here $\tilde{T}_1$, $\tilde{T}_{K+1}$ must be computed by extrapolation,

(c) With $\tilde{\Phi}_k$ and $\tilde{T}_k$ known, geopotential values at mandatory pressures $\Phi_{mand}$ are computed by

$$\Phi_{mand} = \Phi(\bar{Z}) + A(Z_{mand} - \bar{Z}) + \frac{1}{2} B(Z_{mand} - \bar{Z})^2 \quad , \tag{83}$$

where $\Phi(\bar{Z}) = (\Phi_a + \Phi_b)/2 - B(Z_{mand} - \bar{Z})^2/8$ and B, A, $\bar{Z}$ are given as in Eq. (71) except that $p_a$, $p_b$ are now pressures at two adjacent model interfaces between which $p_{mand}$ lies. In the case where $p_{mand} < p_*$, we simply adopt NMC's Shuell method to obtain $\Phi_{mand}$ values at mandatory pressures below the earth's surface.

For values of wind, temperature, and specific humidity at mandatory surfaces, linear interpolation/extrapolation in Z is used:

$$F_{mand} = F_b + \frac{F_a - F_b}{Z_a - Z_b} (Z_{mand} - Z_b) \quad . \tag{84}$$

Here $p_{mand}$ lies between layer pressures $p_a$ and $p_b$, and F represents T, U, V, or Q. For specific humidity we compute $Q_{mand}$ only for cases where $p_{mand} > 300$ mb. Finally, $Q_{mand}$ are to be converted to $RH_{mand}$ using Eq. (77).

### 4.2 Initialization Procedure

The normal-mode initialization of Machenhauer[13] is applied to the initial data following the procedure developed by Ballish.[14] The theoretical background and specific details of the procedure are described by Sela.[15]

We shall confine ourselves to presenting data that show the differences in the basis functions between our model and the NMC model. These variations are due to the differences in sigma structure and horizontal truncation.

---

13. Machenhauer, B. (1977) On the dynamics of gravity oscillations in a shallow water model with applications to normal mode initialization, Beit. Phys. Atmos. 50:253-271.

14. Ballish, A. B. (1980) Initialization Theory and Application to the NMC Spectral Model, PhD Thesis, Dept. of Meteorology, Univ. of Maryland.

15. Sela, J. G. (1982) The NMC Spectral Model, NOAA Technical Report NWS-30, 36 pp.

First of all, as Ballish remarked, there is no a priori reason that the eigenvalues associated with the vertical structure of any model be real. However, their values must be real in order that the normal-mode representation be meaningful. Our experience with a number of samples shows that both the eigenvalues and the eigenvectors are robust in the sense that they remain real and stable with regard to changes in either the sigma structure or the basic temperature profile of the model. Tables 2 and 3 present the sets of eigenvalues for the six-layer and 12-layer models, respectively, with three different basic temperature profiles. Figures 2 through 5 show the eigenvectors corresponding to the four largest eigenvalues of some of the cases included in Tables 2 and 3. Variations of the eigenvalues with structure and profile, and similarities in the profiles of the eigenvectors among the various structures and profiles clearly illustrate these points.

With the rhomboidal truncation M = 15, the matrix of the eigensystem for either symmetric or antisymmetric flow is of order 24 (=3 × 8). The corresponding eigenvectors consist of eight components each of divergence, vorticity, and the composite function, $W = \Phi + RT_0 q$. For a given zonal wavenumber, both the symmetric and antisymmetric flows will generally have 24 distinct eigenvalues and eigenvectors. The only exception is found with m = 0, where the symmetric flow includes 14 gravity modes and two stationary modes, while the antisymmetric flow contains 16 gravity modes. All Rossby modes are degenerate in this case. For $m \neq 0$, of the 24 modes, 16 are gravity modes that are equally divided between eastward- and westward-propagating waves while the remaining eight are the Rossby modes. Faster gravity waves have smaller length scale in the meridional direction, while faster Rossby waves are associated with larger length scale. Table 4 summarizes some of the characteristics of the horizontal normal modes associated with the M = 15, six-layer AFGL model with a $300^{\circ}$ K-isothermal basic temperature profile.

For the experiments reported in Section 5.2, the initialization was applied only to the two largest vertical modes and only to those horizontal modes whose periods are less than 48 hr. The best results were obtained with two iterations.

Table 2. Eigenvalues of Vertical Modes of Six-layer Models ($m^2$ $sec^{-2}$)

| | GL Six-layer | | | Equi-thickness Six-layer | | |
|---|---|---|---|---|---|---|
| | Standard | 270° Isothermal | 300° Isothermal | Standard | 270° Isothermal | 300° Isothermal |
| 1 | 93768 | 104865 | 116516 | 93512 | 104395 | 115994 |
| 2 | 19945 | 28085 | 31206 | 14589 | 21193 | 23547 |
| 3 | 1356 | 3463 | 3848 | 1362 | 3616 | 4017 |
| 4 | 289 | 743 | 826 | 273 | 830 | 923 |
| 5 | 99 | 280 | 311 | 72 | 219 | 144 |
| 6 | 15 | 43 | 48 | 12 | 36 | 40 |

Table 3. Eigenvalues of Vertical Modes of 12-layer Models ($m^2$ $sec^{-2}$)

| | NMC 12-layer | | | Equi-thickness 12-layer | | |
|---|---|---|---|---|---|---|
| | Standard | 270° Isothermal | 300° Isothermal | Standard | 270° Isothermal | 300° Isothermal |
| 1 | 94463 | 106102 | 117891 | 94140 | 105484 | 117204 |
| 2 | 27094 | 33855 | 37616 | 22349 | 28800 | 32000 |
| 3 | 5209 | 9372 | 10413 | 3051 | 6810 | 7567 |
| 4 | 1559 | 3194 | 3549 | 1000 | 2174 | 2415 |
| 5 | 696 | 1470 | 1634 | 361 | 912 | 1013 |
| 6 | 324 | 715 | 794 | 160 | 426 | 474 |
| 7 | 152 | 388 | 431 | 76 | 218 | 242 |
| 8 | 86 | 209 | 233 | 39 | 112 | 125 |
| 9 | 44 | 105 | 116 | 19 | 57 | 64 |
| 10 | 22 | 59 | 66 | 9 | 27 | 30 |
| 11 | 7 | 21 | 24 | 3 | 10 | 11 |
| 12 | 2 | 5 | 6 | 1 | 2 | 2 |

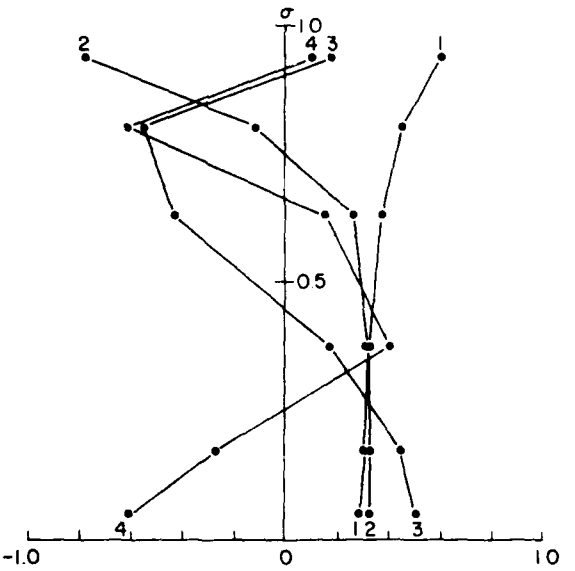


Figure 2. Vertical Profile of the Eigenvectors for the AFGL, Six-layer, 300°K-Isothermal Structure

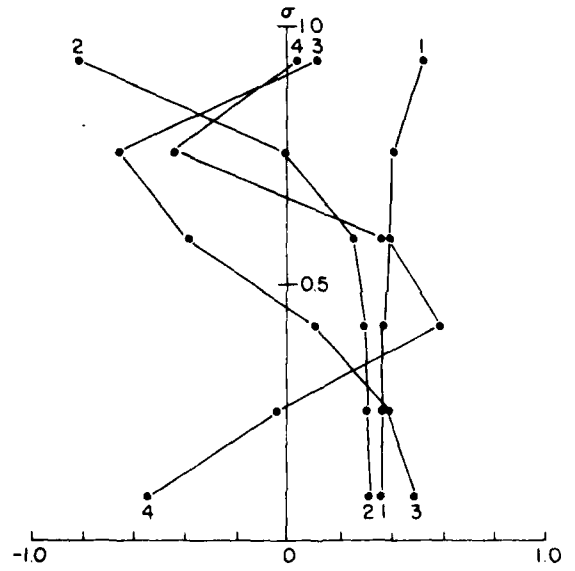


Figure 3. Vertical Profile of the Eigenvectors for an Equi-thickness, Six-layer Standard Structure

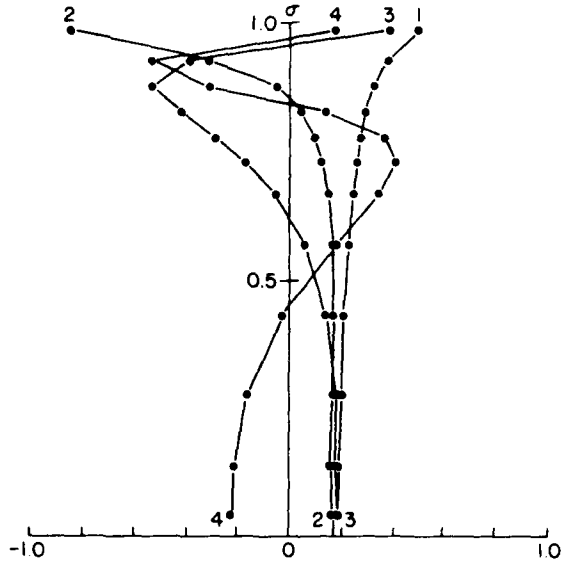


Figure 4. Vertical Profile of the Eigenvectors for the NMC, Twelve-layer, 300°K-Isothermal Structure

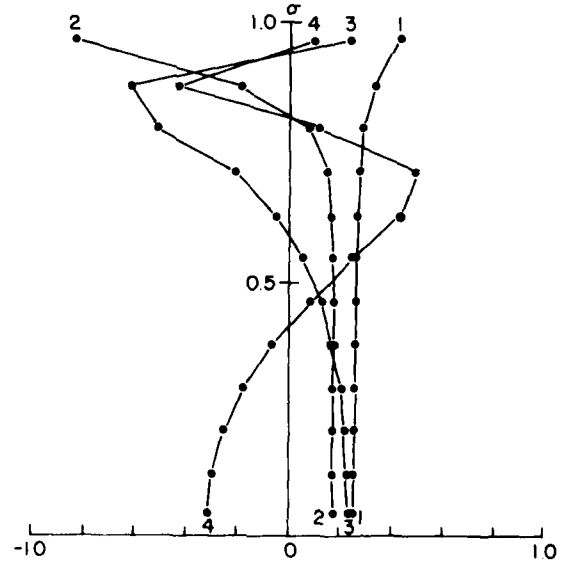


Figure 5. Vertical Profile of the Eigenvectors for an Equi-thickness, Twelve-layer, Standard Structure

Table 4. Some Characteristics of the Horizontal Normal Modes With 16-wave Rhomboidal, AFGL Six-layer Model, and the 300°-K Isothermal Basic Temperature Profile

| Vertical Mode Number | Zonal Wave Number | Period in Hours of | | |
|---|---|---|---|---|
| | | Fastest Gravity Mode | Slowest Gravity Mode | Fastest Rossby Mode |
| 1 | 0 | 2.09 | 18.0 | ∞ |
| | 1 | 1.97 | 29.5 | 27.8 |
| | 5 | 1.58 | 6.07 | 72.9 |
| | 15 | 1.07 | 2.11 | 19.2 |
| 2 | 0 | 4.00 | 26.6 | ∞ |
| | 1 | 3.76 | 38.4 | 31.8 |
| | 5 | 3.04 | 11.8 | 75.0 |
| | 15 | 2.05 | 4.09 | 193 |
| 3 | 0 | 9.36 | 46.0 | ∞ |
| | 1 | 9.00 | 78.7 | 43.0 |
| | 5 | 7.81 | 33.3 | 86.3 |
| | 15 | 5.67 | 11.7 | 196 |
| 4 | 0 | 11.7 | 67.9 | ∞ |
| | 1 | 11.1 | 125 | 101 |
| | 5 | 11.2 | 69.5 | 104 |
| | 15 | 10.1 | 25.4 | 205 |
| 5 | 0 | 12.1 | 88.2 | ∞ |
| | 1 | 11.2 | 163 | 137 |
| | 5 | 12.2 | 109 | 120 |
| | 15 | 12.5 | 41.3 | 216 |
| 6 | 0 | 12.3 | 177 | ∞ |
| | 1 | 11.2 | 242 | 289 |
| | 5 | 12.7 | 246 | 179 |
| | 15 | 14.4 | 104 | 257 |

## 5. RESULTS

In this section we present the results of several time integrations to establish the performance of the low resolution baseline model. In all cases we used a rhomboidal truncation of M = 15 with six unequally-spaced σ layers (see Figure 1 and Table 1). Unless otherwise noted, we used the semi-implicit time scheme with a time step at $\Delta t$ = 60 min. Two types of initial data were used for testing purposes: (a) idealized analytic Rossby-Haurwitz waves and (b) global FGGE level III-A data for the weeks of 15 January 1978 and 16 July 1978.

### 5.1 Forecasts With Analytic Initial Conditions

For the preliminary test of the model's coding and performance, we used the analytic initial conditions suggested by Phillips[16] for a barotropic model and modified for use in a multilayer model as shown by Bourke.[7] The model was initialized with the same flow pattern in all layers. It consisted of a mean zonal flow plus a zonal wavenumber 4 eddy with the streamfunction given by

$$\psi(\lambda,\phi) = \psi_1^0 P_1^0(\sin\phi) + \psi_5^4 P_5^4(\sin\phi)\, e^{4i\lambda} + \psi_5^{4*} P_5^4(\sin\phi)\, e^{-4i\lambda} \quad , \tag{85}$$

where the spectral amplitudes are

$$\psi_1^0 = -a^2 \omega \sqrt{\frac{2}{3}}$$

$$\psi_5^4 = \frac{a^2 \omega}{1890} \sqrt{\frac{2 \cdot 9!}{11}}$$

with $\omega = \frac{\Omega}{10}$ and $\Omega$ is the angular velocity of the earth. Additional specifications of the initial conditions included an isothermal atmosphere with $T_0 = 266.5^{\circ}K$ in all layers, a mean surface pressure of 100 cb, and no topography so that $\Phi_* = 0$ everywhere. The initialization was completed with a non-divergent balance condition obtained from Eq. (24) by initially setting

$$\frac{\partial D_n^m}{\partial t} = \Phi_n^m = 0$$

and then solving for $q_n^m$. In this case, the model was treated as inviscid, adiabatic, and dry (that is, all of the physical parameterizations were turned off).

We note that the analytic barotropic non-divergent solution consists of a zonal wavenumber 4 pattern that preserves its shape and amplitude and rotates from west to east with a phase speed of $9.6^{\circ}$ per day. For the multilayer model, the flow should resemble the barotropic solution for the first few time-steps and then slowly deviate as divergence and vertical shear develop.

In Table 5, we show the amplitude and phase speed of the $\psi_5^4$ mode resulting from two different 72-hr forecasts, one using an explicit time scheme with a time-step of 10 min and the other using the semi-implicit scheme described before.

---

16. Phillips, N.A. (1959) Numerical integrations of the primitive equations on the hemisphere, Mon. Wea. Rev. 87:333-345.

Table 5. Amplitude ($10^7$ $m^2$ $sec^{-1}$) and Phase Speed (Degrees per Day) of the $\psi_5^4$ Mode

| Explicit Time Scheme ($\Delta t$ = 10 min) | | | | | | |
|---|---|---|---|---|---|---|
| | 24 hr | | 48 hr | | 72 hr | |
| $\sigma$ | A | P | A | P | A | P |
| 0.0622 | 3.995 | 9.47 | 3.949 | 9.48 | 3.838 | 9.49 |
| 0.1985 | 3.999 | 9.37 | 3.879 | 9.30 | 3.826 | 9.15 |
| 0.3699 | 3.986 | 9.13 | 3.951 | 8.97 | 3.951 | 8.97 |
| 0.6220 | 4.016 | 8.94 | 4.011 | 8.90 | 4.044 | 8.92 |
| 0.8242 | 4.030 | 8.85 | 4.046 | 8.91 | 4.041 | 8.95 |
| 0.9497 | 4.039 | 8.84 | 4.029 | 8.95 | 3.983 | 8.93 |
| Average | 4.009 | 9.09 | 3.981 | 9.05 | 3.961 | 9.05 |
| Analytic | 4.023 | 9.6 | 4.023 | 9.6 | 4.023 | 9.6 |
| Semi-implicit Time Scheme ($\Delta t$ = 60 min) | | | | | | |
| | 24 hr | | 48 hr | | 72 hr | |
| $\sigma$ | A | P | A | P | A | P |
| 0.0622 | 4.001 | 9.46 | 3.957 | 9.41 | 3.825 | 9.37 |
| 0.1985 | 4.003 | 9.37 | 3.901 | 9.20 | 3.854 | 9.00 |
| 0.3699 | 3.992 | 9.10 | 3.975 | 8.86 | 3.996 | 8.78 |
| 0.6220 | 4.030 | 8.93 | 4.040 | 8.83 | 4.113 | 8.75 |
| 0.8242 | 4.051 | 8.85 | 4.091 | 8.85 | 4.079 | 8.82 |
| 0.9497 | 4.063 | 8.85 | 4.093 | 8.88 | 4.038 | 8.80 |
| Average | 4.020 | 9.08 | 4.010 | 8.97 | 4.002 | 8.89 |

In both cases, we find that the model behaves as expected, that is, the flow resembles the barotropic solution with deviations that increase with time. As noted by Bourke,[7] we also find that the upper layers tend to preserve the phase speed of the barotropic flow while the lower layers tend to preserve the amplitude of the wave. In general, the vertically-averaged amplitude and phase speed both decrease slightly as the forecasts proceed. The small differences between the explicity and semi-implicit results can easily be explained in terms of the known characteristics of each of these time schemes (for example, Kurihara[17]).

17. Kurihara, Y. (1965) On the use of implicit and iterative methods for the time integration of the wave equation, Mon. Wea. Rev. 93:33-46.

Finally, the analytic initialization experiments provide an opportunity to check the conservation properties of the model. For the 72-hr semi-implicit integration, the changes in total energy (sum of kinetic, internal, and gravitational potential), mass, and angular momentum were -0.0034, -0.0035, and -0.162 percent, respectively. For the explicit integration the change in energy was -0.0026 percent. All of these values are considered acceptable and allow us to proceed to the more realistic simulations that include all of the physical parameterizations and use actual data for initial conditions.

### 5.2 Forecasts With Global Data

As was mentioned previously, the data used for the global test forecasts consisted of FGGE level III-A data sets for the weeks beginning 15 January 1978 and 16 July 1978. In view of the limited number of days of data available, the decision was made to run four test forecasts – one for the first 48-hr period of each week and one for the last 48-hr period of each week. This was done in order to test the model on as many synoptically independent cases as possible. While the separation of four days may not be quite enough for synoptic independence, it was the best that could be done under the circumstances. Thus the four test forecasts included two winter cases with 00Z 15 January 1978 and 12Z 19 January 1978 and two summer cases with 00Z 16 July 1978 and 12Z 20 July 1978 as the initial times. We note that in the six-layer, M = 15 rhomboidal configuration with $\Delta t$ = 60 min the model required 83K words of memory and used 18 min of CPU time for each 24 hr of simulation on the CDC 6600.

In the course of evaluating the model's performance, we found it helpful and interesting to assess the relative influences of each of the three components of the model (preprocessing, prognostication, and postprocessing) as shown in Figure 6. It is obvious that the preprocessing and postprocessing are purely static while the prognostication includes both static and dynamic changes. If the errors accrued in the static transformation during the processing stages were statistically independent of those produced during the prognostication the total error variance of the model would be the sum of the two partial error variances. In practice, however, because of the presence of common elements in both physical assumptions and mathematical procedures among different components we do not expect a strict statistical independence between the processing parts and the prognostic part. Nonetheless, it was thought that such a partition might shed a light into the composition and nature of the model performance. Toward this end, the performance was measured by the RMSD between the model-produced values and the corresponding analyzed or "truth" values at the grid points. Thus,

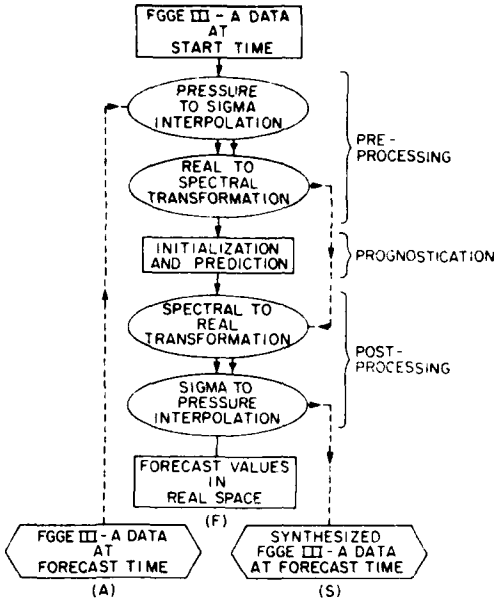


Figure 6. Schematic Diagram of Model Evaluation

$$\text{RMSD} = \left( \frac{1}{2I} \sum_{j=1}^{J} \sum_{i=1}^{I} (M_{ij} - T_{ij})^2 W_j \right)^{1/2} ,$$

where $M_{ij}$ and $T_{ij}$ are the model-produced and "truth" values at grid point (i, j) in which i = 1, 2, ..., I and j = 1, 2, ..., J are the longitudinal and latitudinal indices, respectively, and $W_j$ is the Gaussian weight at latitude j.

For the total performance of the model, the values of $M_{ij}$ were taken from the model forecast and $T_{ij}$ were the values interpolated from the FGGE III-A data set to the Gaussian grid, hereafter referred to as the analyzed values. For the performance of the processing parts, $M_{ij}$ were synthesized from the analyzed values at the time of verification by putting the latter through the preprocessing and postprocessing parts while bypassing the prognostication of the model. Finally, the performance of the prognostication is represented by the RMSD between the model-forecast values and the synthesized values. A table of global performances for vector wind, temperature, and height at three different pressure levels summarizes the model evaluation in each of the four test runs (Table 6 through Table 9). In these tables the letters A, S, F refer to the analyzed, synthesized, and forecasted fields, respectively.

Table 6. Performance (RMS Differences)

| 15 January 1978, 00Z | | | | | | | |
|---|---|---|---|---|---|---|---|
| Level (mb) | Pair | V(m sec$^{-1}$) | | T ($^{o}$K) | | Z (m) | |
| | | 24 hr | 48 hr | 24 hr | 48 hr | 24 hr | 48 hr |
| 850 | (F,A) | 5.4 | 6.8 | 2.6 | 3.6 | 31.6 | 42.2 |
| | (S,A) | 2.5 | 2.5 | 1.7 | 1.7 | 9.9 | 10.4 |
| | (F,S) | 4.8 | 6.4 | 2.4 | 3.4 | 31.0 | 41.7 |
| 500 | (F,A) | 6.7 | 9.0 | 1.9 | 2.7 | 41.5 | 57.3 |
| | (S,A) | 3.6 | 3.7 | 1.7 | 1.6 | 12.1 | 12.7 |
| | (F,S) | 5.5 | 7.9 | 1.4 | 2.3 | 40.4 | 56.9 |
| 250 | (F,A) | 11.3 | 14.6 | 4.4 | 4.8 | 58.8 | 88.7 |
| | (S,A) | 5.5 | 5.5 | 2.8 | 2.6 | 14.2 | 13.6 |
| | (F,S) | 8.6 | 12.2 | 2.3 | 3.0 | 56.5 | 86.8 |

Table 7. Performance (RMS Differences)

| 19 January 1978, 12Z | | | | | | | |
|---|---|---|---|---|---|---|---|
| Level (mb) | Pair | V (m sec$^{-1}$) | | T ($^{o}$K) | | Z (m) | |
| | | 24 hr | 48 hr | 24 hr | 48 hr | 24 hr | 48 hr |
| 850 | (F,A) | 5.3 | 6.7 | 2.5 | 3.4 | 28.8 | 37.0 |
| | (S,A) | 2.5 | 2.8 | 1.6 | 1.9 | 9.1 | 10.3 |
| | (F,S) | 4.6 | 6.0 | 2.2 | 3.3 | 28.4 | 36.8 |
| 500 | (F,A) | 7.1 | 8.7 | 2.0 | 2.6 | 38.4 | 50.7 |
| | (S,A) | 3.7 | 3.7 | 1.7 | 1.5 | 10.4 | 12.0 |
| | (F,S) | 5.8 | 7.6 | 1.5 | 2.3 | 38.0 | 50.2 |
| 250 | (F,A) | 11.7 | 13.9 | 4.3 | 4.8 | 57.1 | 81.8 |
| | (S,A) | 5.9 | 5.5 | 2.8 | 2.8 | 14.0 | 13.5 |
| | (F,S) | 8.8 | 11.6 | 2.2 | 2.8 | 54.8 | 79.8 |

Table 8. Performance (RMS Differences)

| 16 July 1978, 00Z | | | | | | | |
|---|---|---|---|---|---|---|---|
| Level (mb) | Pair | V (m sec$^{-1}$) | | T ($^{o}$K) | | Z (m) | |
| | | 24 hr | 48 hr | 24 hr | 48 hr | 24 hr | 48 hr |
| 850 | (F,A) | 4.7 | 6.8 | 2.3 | 3.2 | 25.7 | 41.7 |
| | (S,A) | 2.3 | 2.5 | 1.6 | 1.5 | 9.6 | 8.6 |
| | (F,S) | 4.1 | 6.2 | 2.0 | 2.9 | 25.3 | 41.2 |
| 500 | (F,A) | 6.0 | 8.6 | 2.1 | 2.5 | 34.7 | 55.4 |
| | (S,A) | 3.1 | 3.4 | 1.6 | 1.6 | 11.1 | 11.0 |
| | (F,S) | 5.1 | 7.8 | 1.4 | 2.1 | 34.0 | 55.0 |
| 250 | (F,A) | 10.8 | 14.2 | 4.4 | 4.7 | 55.4 | 83.8 |
| | (S,A) | 5.7 | 6.3 | 3.0 | 3.0 | 15.0 | 15.5 |
| | (F,S) | 7.9 | 11.3 | 2.2 | 2.6 | 53.0 | 81.9 |

Table 9. Performance (RMS Differences)

| 20 July 1978, 12Z | | | | | | | |
|---|---|---|---|---|---|---|---|
| Level (mb) | Pair | V (m sec$^{-1}$) | | T ($^{o}$K) | | Z(m) | |
| | | 24 hr | 48 hr | 24 hr | 48 hr | 24 hr | 48 hr |
| 850 | (F,A) | 5.0 | 6.3 | 2.7 | 3.1 | 24.6 | 37.7 |
| | (S,A) | 2.3 | 2.1 | 1.5 | 1.5 | 9.4 | 8.8 |
| | (F,S) | 4.5 | 5.9 | 2.5 | 3.1 | 24.1 | 37.1 |
| 500 | (F,A) | 6.2 | 8.1 | 2.1 | 2.5 | 37.7 | 52.2 |
| | (S,A) | 3.3 | 3.4 | 1.6 | 1.6 | 10.7 | 9.8 |
| | (F,S) | 5.2 | 7.1 | 1.6 | 2.4 | 37.2 | 52.1 |
| 250 | (F,A) | 11.0 | 12.8 | 4.4 | 4.8 | 59.4 | 86.1 |
| | (S,A) | 6.2 | 6.2 | 3.0 | 3.0 | 15.3 | 15.2 |
| | (F,S) | 7.9 | 10.4 | 2.2 | 2.5 | 57.4 | 84.5 |

Three features common to all runs seem to stand out well. First, the total MSD are approximately equal to the sum of that due to the processings and that due to the prognostication. Second, the performance of the processing is qualitatively invariant with respect to time and case, indicating that the measure at the global level is insensitive to the synoptic details. The last feature that follows as a combined result of the previous two characteristics is that the degradation with time of the total model performance is due mostly to the prognostication. The values of performance are comparable in magnitudes with the statistics of other current operational* and research[2] models.

For a qualitative assessment of the model's performance, in Figure 7 we show the analyzed 1000- and 500-mb heights for 00Z 15 January-17 January and the corresponding 24- and 48-hr forecasts (16 January and 17 January, respectively) for the Northern Hemisphere. In general, the results are as might be expected based on model performance reported by other researchers using comparable models.[1,2,3] At 24 hr (Figures 7b and 7c) the model is able to correctly forecast the location and movement of the major surface systems and the 500 mb troughs and ridges. At 48 hr (Figures 7d and 7e) the global patterns are predicted reasonably well but phase errors start to become noticeable. Also, a major problem of a low resolution model is its inability to accurately treat smaller scale features such as cutoff lows and sharply defined fronts.

## 6. CONCLUSION

The formulation of the baseline version of the AFGL moist global model has been described in detail. It is patterned after the NMC spectral model.[3,15] The numerical methods in the model include spectral representation in the horizontal, the Arakawa vertical differencing scheme, and the semi-implicit time scheme. The data processing, normal-mode initialization, and the parameterized physical processes have all been adapted from the NMC model. Test forecasts for a limited number of cases indicate that the model performs as well as other comparable large-scale models.

### 6.1 Future Research

It should be emphasized that the model documented in this report is a baseline version and is therefore only a starting point for additional research. One of the major goals of our future effort is to provide the model with a useful cloud

*NMC global spectral model and GWC AWSPE, private communication.

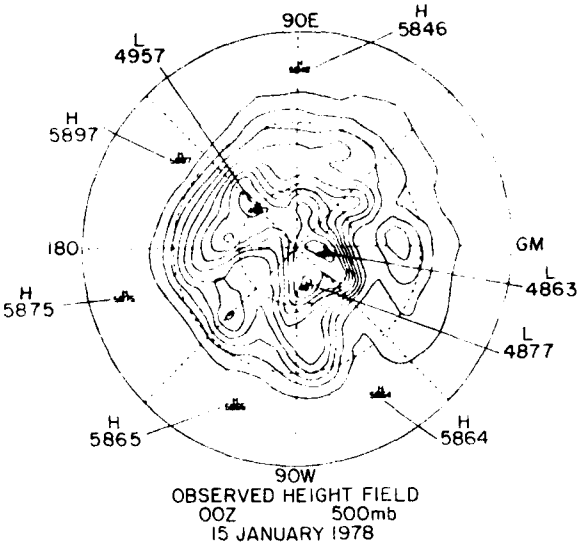


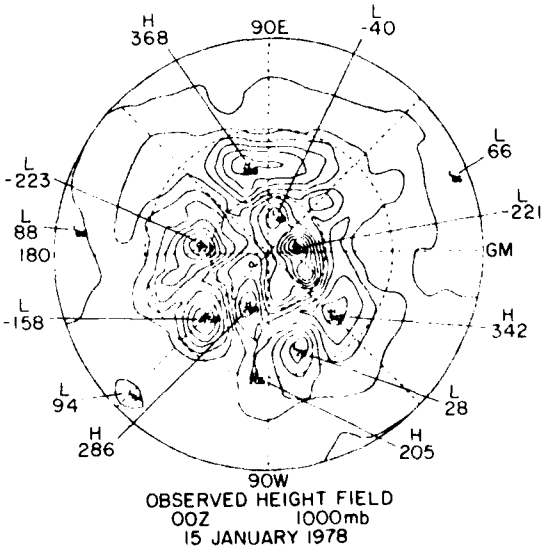


Figure 7a. Analyzed Height Fields for 1000 mb and 500 mb for 00Z 15 January 1978 (Initial Fields)

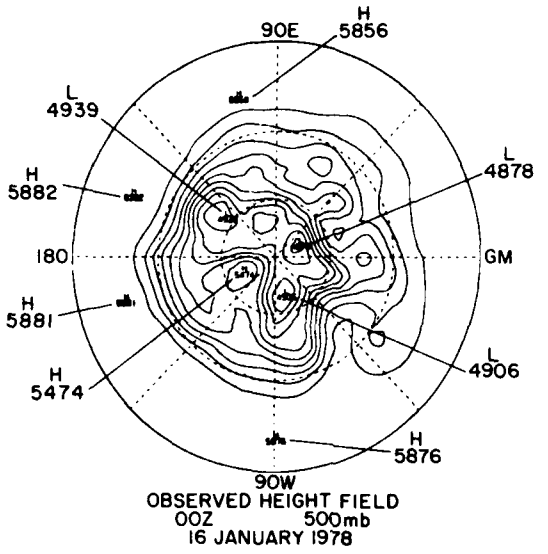


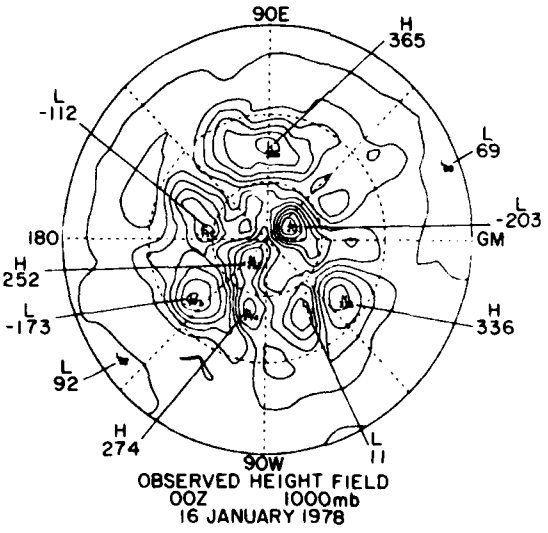


Figure 7b. Analyzed Height Fields for 1000 mb and 500 mb for 00Z 16 January 1978

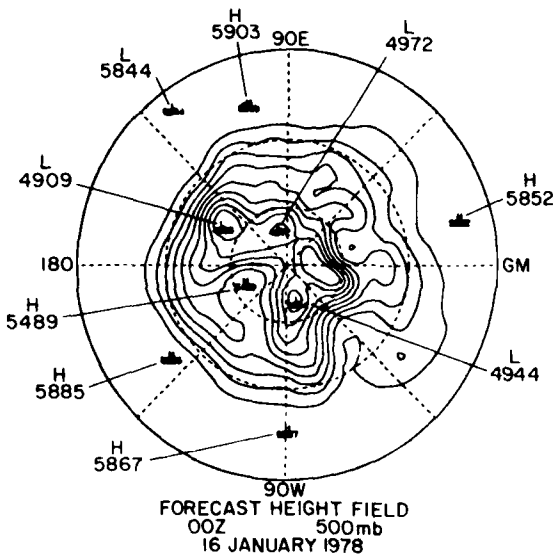


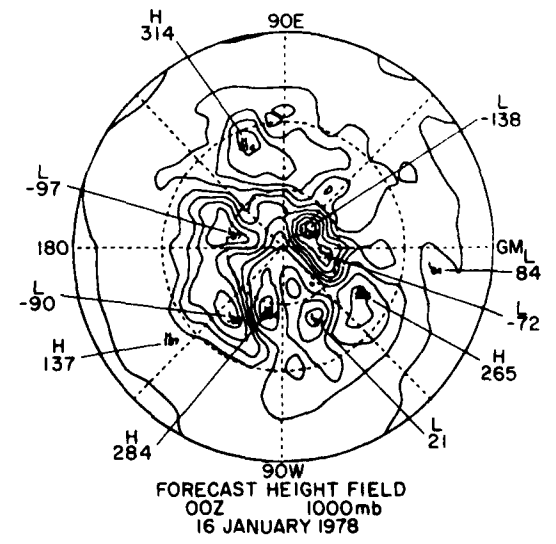


Figure 7c. Height Fields for 24-hr Forecast for 00Z 16 January 1978

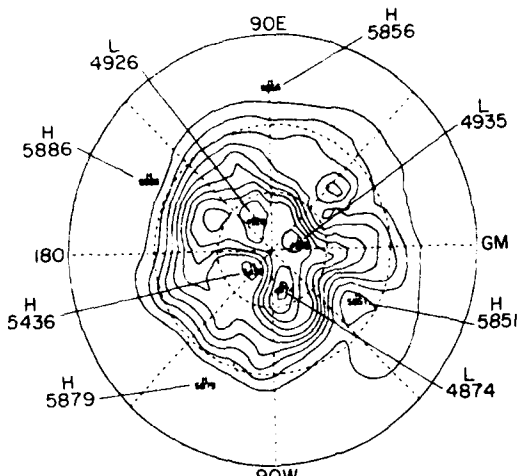


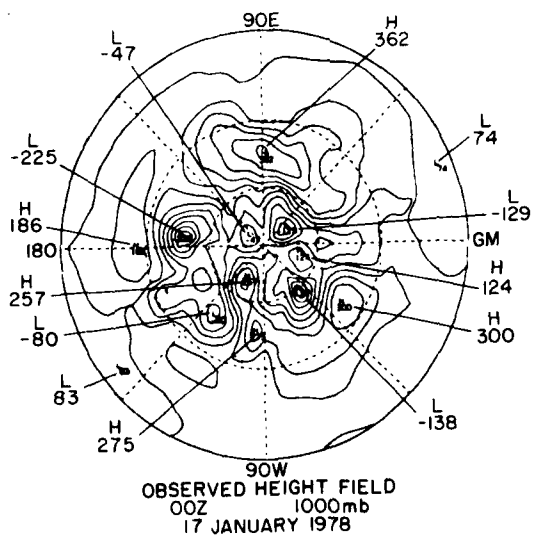


Figure 7d. Analyzed Height Fields for 1000 mb and 500 mb for 00Z 17 January 1978

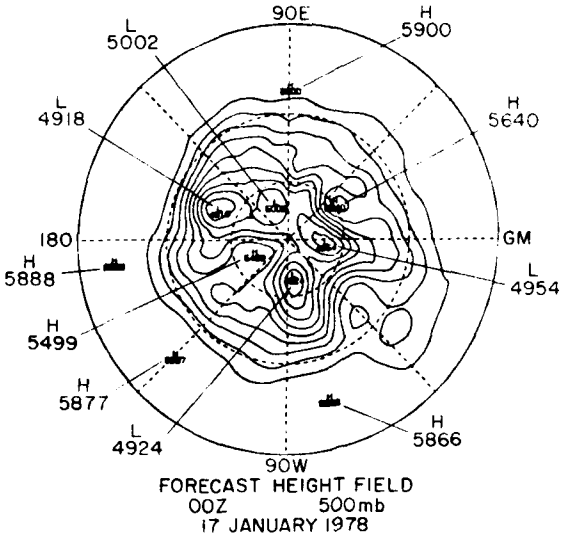


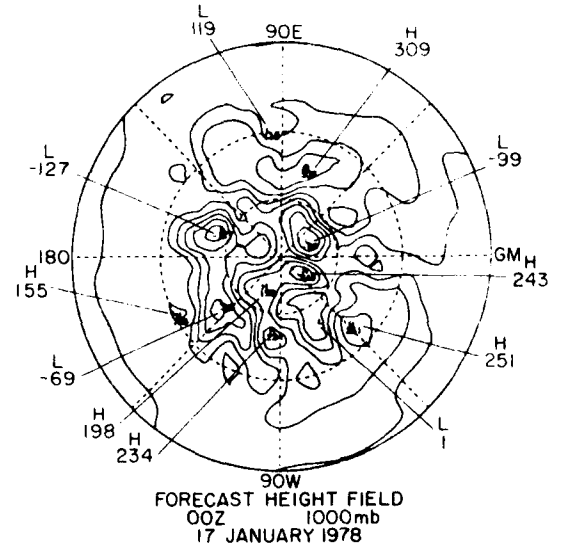


Figure 7e. Height Fields for 48-hr Forecast for 00Z 17 January 1978

forecasting capability. Some of the preliminary steps and procedures necessary for this have already been described by Mitchell. [18]

Success in this area will require major changes and improvements in all aspects of the baseline model:

(a) In the area of dynamics and numerical methods, we are currently working on expanding the resolution of the model (at least 12 layers with M = 30) as well as vectorizing the code for efficient processing on the CRAY-1. We are also considering alternative and potentially more accurate numerical solutions of the hydrostatic equation.

(b) Data processing, including analysis and initialization, is one area that is currently receiving substantial attention throughout the meteorological community. For our model, an effort is under way to develop a scheme that combines optimal interpolation analysis and nonlinear normal mode initialization. Other research in the processing procedures will focus on improving the pressure-to-sigma and sigma-to-pressure interpolation schemes to make them more accurate and consistent with the vertical structure of the forecast model.

(c) The parameterized physics in the model will also be completely changed. Efforts are currently in progress to develop improved schemes for boundary-layer and moisture physics. In addition, a radiation package will be added to the model.

(d) Finally, an effort is being made to develop preliminary software that will produce derived cloud forecasts based on the model-forecasted moisture field.

---

18. Mitchell, K.E. (1982) Cloud Forecast Fields Comparison Test, AFGWC Technical Note 82/003, 66 pp.

## References


1. Hoskins, B.J., and Simmons, A.J. (1975) A multi-layer spectral model and the semi-implicit method, Quart. J. Roy. Meteorol. Soc. 101:637-655.
2. Bourke, W., McAvaney, B., Puri, K., and Thurling, R. (1977) Spectral methods for atmospheric modeling, Methods in Computational Physics, Vol. 17.
3. Sela, J. (1980) Spectral modeling at the National Meteorological Center, Mon. Wea. Rev. 108:1279-1292.
4. Eliasen, E., Machenauer, B., and Rasmussen, E. (1970) On a Numerical Method for Integration of the Hydrodynamical Equations With a Spectral Representation of the Horizontal Fields. Inst. of Theor. Meteorology, Univ. of Copenhagen, Report No. 2.
5. Orszag, S.A. (1970) Transform method for calculation of vector coupled sums: Application to the spectral form of the vorticity equation, J. Atmos. Sci. 27:890-895.
6. Phillips, N.A. (1957) A coordinate system having some special advantages for numerical forecasting, J. Meteorol. 14:184-185.
7. Bourke, W. (1974) A multi-level spectral model. I. Formulation and hemispheric integrations, Mon. Wea. Rev. 102:687-701.
8. Arakawa, A., and Mintz, Y. (1974) The UCLA Atmospheric Circulation Model, Dept. of Meteorology, University of California.
9. Silberman, J.S. (1954) Planetary waves in the atmosphere, J. Meteorol. 11:27-34.
10. Robert, A. (1979) The semi-implicit method, Numerical Methods Used in Atmospheric Models, Vol. 2. GARP Publication Series, No. 17. Geneva, WMO, pp. 419-439.
11. Kuo, H.L. (1965) On formation and intensification of tropical cyclones through latent heat release by cumulus convection, J. Atmos. Sci. 22:40-63.

12. Phillips, N.A. (1979) The Nested Grid Model, NOAA Technical Report NWS-22, 79 pp.

13. Machenhauer, B. (1977) On the dynamics of gravity oscillations in a shallow water model with applications to normal mode initialization, Beit. Phys. Atmos. 50:253-271.

14. Ballish, A.B. (1980) Initialization Theory and Application to the NMC Spectral Model, PhD Thesis, Dept. of Meteorology, Univ. of Maryland.

15. Sela, J.G. (1982) The NMC Spectral Model, NOAA Technical Report NWS-30, 36 pp.

16. Phillips, N.A. (1959) Numerical integrations of the primitive equations on the hemisphere, Mon. Wea. Rev. 87:333-345.

17. Kurihara, Y. (1965) On the use of implicit and iterative methods for the time integration of the wave equation, Mon. Wea. Rev. 93:33-46.

18. Mitchell, K.E. (1982) Cloud Forecast Fields Comparison Test, AFGWC Technical Note 82/003, 66 pp.

# Appendix A

## Numerical Values of Physical Constants

| | |
|---|---|
| g | $9.8\ m\ s^{-1}$ |
| a | $6.371 \times 10^{6}\ m$ |
| $\Omega$ | $7.292116 \times 10^{-5}\ s^{-1}$ |
| R for dry air | $287.05\ J\ kg^{-1}\ K^{-1}$ |
| $C_p$ for dry air | $1005\ J\ kg^{-1}\ K^{-1}$ |
| $\varepsilon$ ratio of molecular weight of water to that of air | 0.622 |
| R for water vapor | $461.5\ J\ kg^{-1}\ K^{-1}$ |
| L of condensation | $2.51 \times 10^{6}\ J\ kg^{-1}$ |
| L of sublimation | $2.835 \times 10^{6}\ J\ kg^{-1}$ |
| specific heat of liquid water | $4187\ J\ kg^{-1}\ K^{-1}$ |
| specific heat of ice | $1922\ J\ kg^{-1}\ K^{-1}$ |
| $C_p$ for water vapor | $1876.5\ J\ kg^{-1}\ K^{-1}$ |

# Appendix B

## Derivation of the Semi-Implicit Time Integration Scheme

We shall be concerned only with the coupled system that consists of the divergence, thermodynamic, and surface pressure tendency equations. We first substitute for $T = T_0 + T'$ and separate the linear divergence terms from the nonlinear terms in the thermodynamic equation. Next, we transpose all the linear terms in Eqs. (24), (25), and (27) to the left-hand side and write them, for each (m,n), as

$$\frac{\partial \underset{\sim}{D}}{\partial t} - \frac{n(n+1)}{a^2}(\underset{\sim}{\Phi} + Rq\underset{\sim}{T}_0) = \underset{\sim}{x} \tag{B1}$$

$$\frac{\partial \underset{\sim}{T}}{\partial t} + C\underset{\sim}{D} = \underset{\sim}{y} \tag{B2}$$

$$\frac{\partial q}{\partial t} + \underset{\sim}{r}\,\underset{\sim}{D} = z \quad . \tag{B3}$$

Here the components of each of the column vectors $\underset{\sim}{D}$, $\underset{\sim}{\Phi}$, $\underset{\sim}{T}$, $\underset{\sim}{x}$, and y are the K layer values of the parameters involved; the symbols $\underset{\sim}{x}$, $\underset{\sim}{y}$, and z represent all of the nonlinear terms on the right-hand side; and the reference to (m,n) has been dropped for brevity. The column vector $\underset{\sim}{T}_0$, the row vector $\underset{\sim}{r}$, and the $K \times K$ matrix C are independent of the time and (m,n). They are given by

$$\underset{\sim}{T}_0 = (T_{01},\ T_{02},\ \ldots,\ T_{0K})^T$$

$$\underset{\sim}{r} = (r_1,\ r_2,\ \ldots,\ r_K)$$

$$C = \left\{ \begin{array}{l} \nu_k r_j,\ j=1,\ k-1 \\ \mu_k r_j,\ j=k \\ \lambda_k r_j,\ j=k+1,\ K \end{array} \right\} \quad k=1,\ K \quad ,$$

where

$$r_k = \tilde{\sigma}_{k+1} - \tilde{\sigma}_k$$

$$\lambda_k = \kappa T_{0,k} - (\tilde{\sigma}_k H_k + \tilde{\sigma}_{k+1} G_k)/r_k$$

$$\mu_k = \lambda_k + G_k/r_k$$

$$\nu_k = \mu_k + H_k/r_k$$

$$G_k = \left\{ T_{0,k} - \left( \frac{\sigma_k}{\sigma_{k+1}} \right)^{\kappa} T_{0,k+1} \right\} /2 \quad .$$

$$H_k = \left\{ T_{0,k-1} \left( \frac{\sigma_k}{\sigma_{k-1}} \right)^{\kappa} - T_{0,k} \right\} /2 \quad .$$

Next, we write Eqs. (43) and (46) in matrix form

$$\underset{\sim}{\Phi} = A\ \underset{\sim}{T} + \Phi_* \underset{\sim}{e} \quad , \tag{B4}$$

where A is a $K \times K$ matrix whose elements are functions of $\sigma_k$ and $r_k$; and $\underset{\sim}{e}$ is a unit vector. Eliminating $\underset{\sim}{\Phi}$ between (B1) and (B4), we have

$$\frac{\partial \underset{\sim}{D}}{\partial t} - \frac{n(n+1)}{a^2} (A\ \underset{\sim}{T} + Rq\ \underset{\sim}{T}_0) = \underset{\sim}{x} + \frac{n(n+1)}{a^2} \Phi_* \underset{\sim}{e} \quad . \tag{B5}$$

We now let

$$\underset{\sim}{T} = \alpha\underset{\sim}{T}^{+}(1 - \alpha)\underset{\sim}{T}^{-}$$

$$\underset{\sim}{D} = \alpha\underset{\sim}{D}^{+}(1 - \alpha)\underset{\sim}{D}^{-}$$

$$q = \alpha q^{+}(1 - \alpha)q^{-} \tag{B6}$$

for the undifferentiated linear terms in Eqs. (B2), (B3), and (B5) and we approximate the time derivatives by centered-differencing,

$$\frac{\partial \underset{\sim}{F}}{\partial t} \approx \frac{\underset{\sim}{F}^{+} - \underset{\sim}{F}^{-}}{2\Delta t} \quad . \tag{B7}$$

Equations (B5), (B2), and (B3) may then be written as

$$\underset{\sim}{D}^{+} - 2\Delta t\,\alpha\,\frac{n(n+1)}{a^2}(A\underset{\sim}{T}^{+} + Rq^{+}\underset{\sim}{T}_0) = \underset{\sim}{D}^{-} + 2\Delta t\left(\underset{\sim}{x} + \frac{n(n+1)}{a^2}\,\underset{\sim}{\phi}_{*}\,e\right)$$

$$+ 2\Delta t(1 - \alpha)\,\frac{n(n+1)}{a^2}\,(A\underset{\sim}{T}^{-} + Rq^{-}\underset{\sim}{T}_0) \quad , \tag{B8}$$

$$\underset{\sim}{T}^{+} = \underset{\sim}{T}^{-} - 2\Delta t\alpha C\underset{\sim}{D}^{+} - 2\Delta t(1 - \alpha)C\underset{\sim}{D}^{-} + 2\Delta t\underset{\sim}{y} \quad , \tag{B9}$$

$$q^{+} = q^{-} - 2\Delta t[\alpha\underset{\sim}{r}\underset{\sim}{D}^{+} + (1 - \alpha)\underset{\sim}{r}\underset{\sim}{D}^{-}] + 2\Delta tz \quad . \tag{B10}$$

Let I be the identity matrix of order K. Elimination of $T^{+}$ and $q^{+}$ in Eq. (B8) leads to the linear system

$$\left[I + (2\Delta t\alpha)^2\,\frac{n(n+1)}{a^2}\,(AC + R\underset{\sim}{T}_0\underset{\sim}{r})\right]\underset{\sim}{D}^{+} =$$

$$\left[I - \frac{1 - \alpha}{\alpha}\,(2\Delta t\alpha)^2\,\frac{n(n+1)}{a^2}\,(AC + R\underset{\sim}{T}_0\underset{\sim}{r})\right]\underset{\sim}{D}^{-} +$$

$$2\Delta t\underset{\sim}{x} + \frac{n(n+1)}{a^2}\,[\Phi_{*}\underset{\sim}{\varepsilon} + A(\underset{\sim}{T}^{-} + 2\Delta t\alpha\underset{\sim}{y}) + R(q^{-} + 2\Delta t\alpha z)\underset{\sim}{T}_0 \quad , \tag{B11}$$

which can be solved for $\underset{\sim}{D}^+$. Once $\underset{\sim}{D}^+$ values are computed, $\underset{\sim}{T}^+$ and $q^+$ are easily obtained by solving (B9) and (B10).

## List of Symbols

| | |
|---|---|
| a | radius of the earth |
| f | Coriolis parameter |
| g | gravity |
| i | $\sqrt{-1}$ |
| j, k, l | indices |
| $\underset{\sim}{k}$ | vertical unit vector |
| m | order of spherical harmonic (superscript) |
| n | degree of spherical harmonic (subscript) |
| p | pressure |
| $p_*$ | surface pressure |
| q | $\ln p_*$ |
| t | time |
| u, v | eastward and northward components of velocity |
| A, B | nonlinear advection terms |
| $C_p$ | specific heat at constant pressure |
| D | horizontal divergence |
| E | kinetic energy |

| | |
|---|---|
| $H$ | diabatic heating |
| $H_n^m$ | meridional derivative of the associated Legendre function |
| $I$ | nonlinear term in the thermodynamic equation |
| $J$ | nonlinear term in the moisture equation |
| $K$ | number of vertical layers |
| $L_v$ | latent heat of condensation of water vapor |
| $M$ | truncation value of m |
| $N$ | truncation value of n |
| $P_n^m$ | associated Legendre function of order m and degree n |
| $Q$ | specific humidity |
| $R$ | gas constant for dry air |
| $T$ | temperature |
| $T_0$ | basic state temperature |
| $U, V$ | pseudo-velocity = $u \cos \phi$, $v \cos \phi$ |
| $W_j$ | Gaussian weight |
| $Y_n^m$ | spherical harmonic of order m and degree n |
| $\zeta$ | relative vorticity |
| $\eta$ | absolute vorticity |
| $\theta$ | potential temperature |
| $\kappa$ | $R/C_p$ |
| $\lambda$ | longitude |
| $\mu$ | $\sin \phi$ |
| $\nu$ | diffusion coefficient |
| $\sigma$ | vertical coordinate |
| $\dot{\sigma}$ | vertical velocity = $\frac{d\sigma}{dt}$ |
| $\varepsilon$ | ratio of molecular weight of water vapor to that of air |
| $\phi$ | latitude |
| $\chi$ | velocity potential |
| $\psi$ | streamfunction |

| | |
|---|---|
| $\Phi$ | geopotential |
| $\Phi_*$ | surface geopotential |
| $\Omega$ | angular velocity of the earth's rotation |
| $(\ )_n^m$ | spherical harmonic coefficient of order m and degree n |
| $(\overline{\ })^\sigma$ | vertical integral |
| $(\ )_k$ | layer value |
| $(\tilde{\ })_k$ | level (interface) value |
| $(\underset{\sim}{\ })$ | vector |